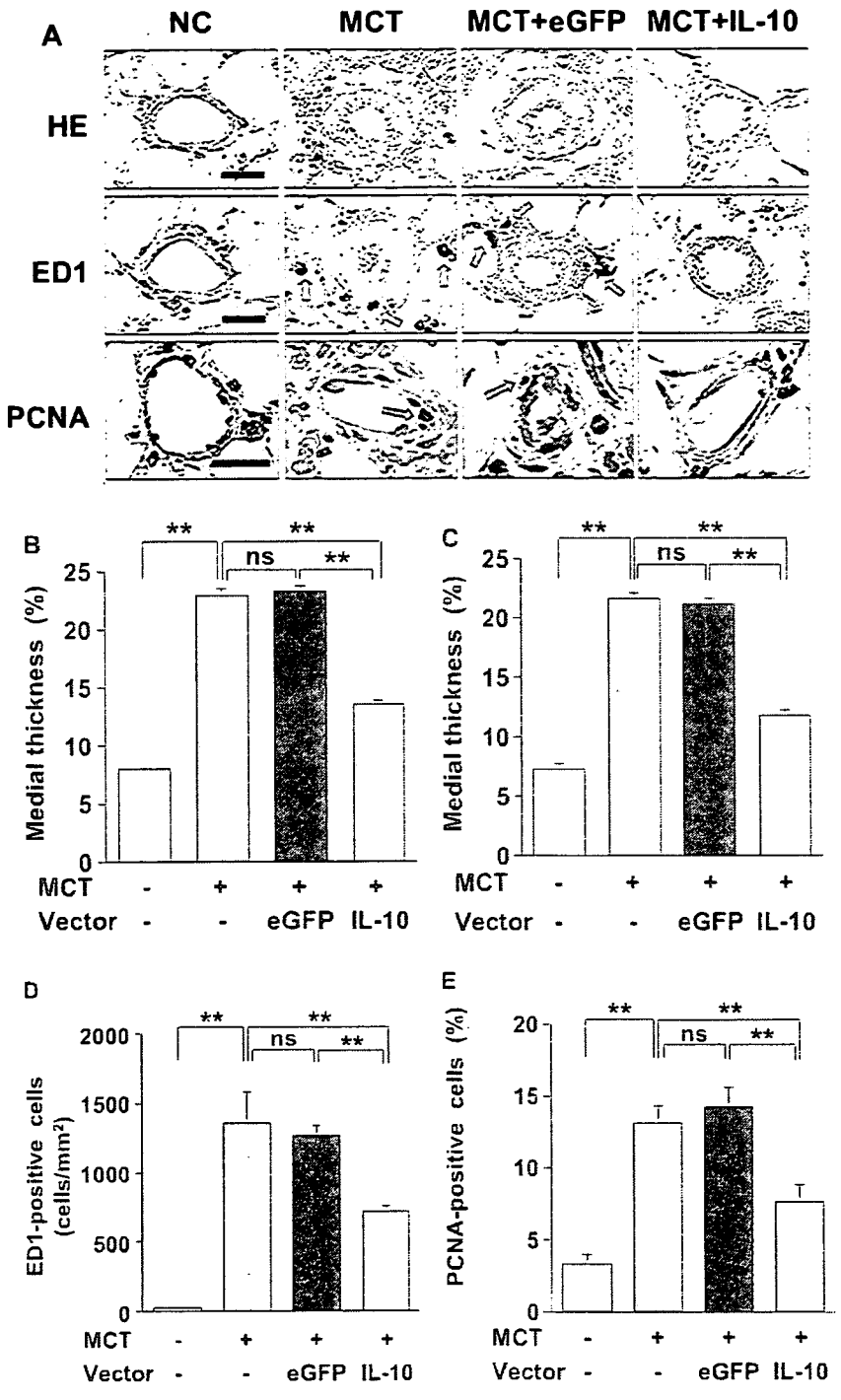

Figure 3. Antiinflammatory and antiproliferative effects of IL-10 on the remodeled pulmonary artery (PA). The 7-week-old Wistar rats were treated with MCT 4 weeks after vector injection. Representative cross-sectional views of the peripheral PAs stained with HE or immunohistochemistry (ED1 or PCNA) 4 weeks after MCT treatment (A; original magnification ×1000, Scale bar=20 μm). Blue arrows indicate ED-1–positive cells and red arrows, PCNA-positive cells. Quantification of percent medial thickness for vessels 25 to 50 μm (B) and 51 to 100 μm (C) in external diameter. Quantitative analysis of the number of perivascular macrophages (ED-1–positive cells, D) and proliferating vascular cells (PCNA-positive cells, E). Data represent mean SEM (n=5 animals per group, $^{**}P<0.01$). ns indicates not statistically significant.

ported. Evidence of right heart failure is involved in the mortality of MCT-PAH rats. In this study, all rats treated with a lethal dose of MCT exhibited symptoms of right heart failure such as pleural effusion and body weight decrease. In the setting of severe PAH and right heart failure, cytokine networks may orchestrate disease progression. Thus, blockades of multiple inflammatory signals might be responsible for the prosurvival effect of IL-10.

IL-10 has gained significant attention because of its suppressive influence on inflammatory and proliferative vasculopathy. The IL-10 receptor is expressed on vascular smooth muscle cells (VSMCs). IL-10 inhibits inflammation and VSMC proliferation in arterial remodeling after balloon injury or transplant rejection.[12,13] Consistent with previous studies using MCT-PAH,[6,7] we demonstrate that increased levels of TGF-β_1 and IL-6 are related to PASMC proliferation and PA remodeling progression. Although treatment with IL-10 alone caused no significant effects on PASMC proliferation,[27] IL-10 significantly inhibited the lung TGF-β_1 expression and TGF-β_1-induced PASMC proliferation. TGF-β_1 enhances PASMC proliferation of idiopathic PAH patients but not that of normal subjects or secondary PAH patients.[28]

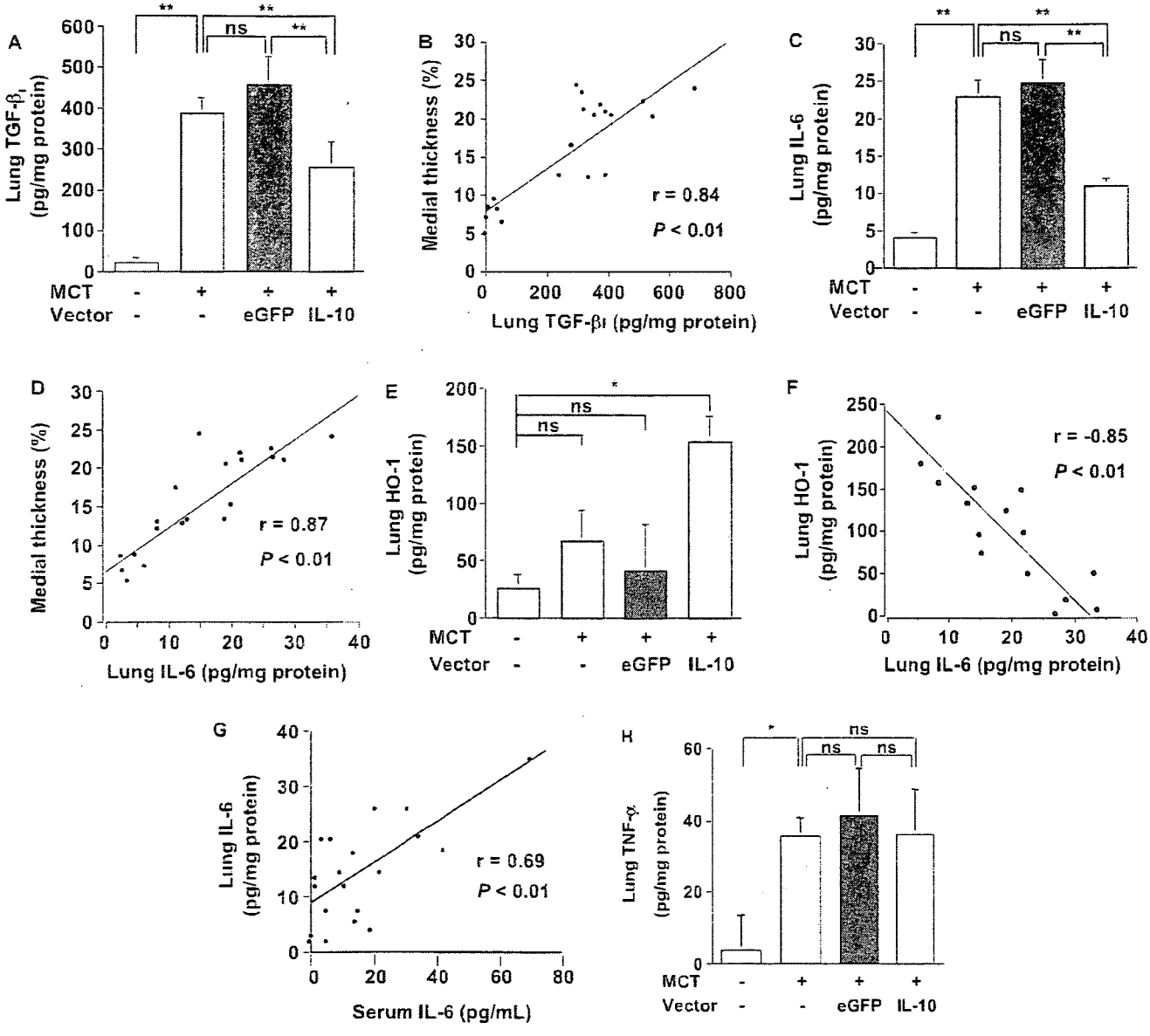

Figure 4. Effects of IL-10 on expression of transforming growth factor-β_1 (TGF-β_1), IL-6, heme oxygenase-1 (HO-1), and tumor necrosis factor-α (TNF-α) in the lung. The 7-week-old Wistar rats were treated with MCT 4 weeks after vector injection. Concentrations of active TGF-β_1 (A), IL-6 (C), HO-1 (E), and TNF-α (H) in the lung extracts were detected using ELISA 4 weeks after MCT treatment. Data represent mean ± SEM (n=5 animals per group; $^*P<0.05$, $^{**}P<0.01$). ns indicates not statistically significant. Correlation between the percent medial thickness and lung levels of TGF-β_1 (B) or IL-6 (D) in rats (groups: NC, MCT, MCT+eGFP, or MCT+IL-10; n=5 animals per group; $r=0.84$, $P<0.01$ and $r=0.87$, $P<0.01$, respectively). Correlation between the HO-1 and IL-6 (F) levels in the rat lung (groups: MCT, MCT+eGFP, or MCT+IL-10; n=5 animals per group; $r=-0.85$, $P<0.01$). Correlation between the lung and serum IL-6 levels (G) in rats (groups: NC, MCT, MCT+eGFP, or MCT+IL-10; n=5 animals per group; $r=0.69$, $P<0.01$).

Additionally, TGF-β_1 is accumulated in the hypertrophic PA of both human PAH and MCT-PAH[29,30] and exacerbates PA remodeling.[31]

IL-6, a multifunctional proinflammatory cytokine, acts as a strong mitogen to promote VSMC proliferation.[11] Macrophage infiltration is a hallmark of PAH progression, and activated macrophages produce substantial amounts of IL-6 in MCT-PAH rats.[6,32] In this study, IL-10 treatment inhibited perivascular macrophage infiltration and the lung IL-6 expression in vivo but not IL-6-induced PASMC proliferation in vitro. These results suggest that IL-10 may attenuate IL-6 function indirectly through the decreased accumulation of perivascular macrophages and IL-6. Furthermore, the serum IL-6 levels significantly correlated with the lung IL-6 levels. Because serum IL-6 level reflects the disease activity of idiopathic PAH, it can be a useful biomarker of antiinflammation therapy of PAH. On the other hand, IL-10 did not affect the MCT-induced TNF-α expression in the lung. However, previous studies demonstrated that IL-10 prevents TNF-α–induced VSMC proliferation in vitro.[27] These observations suggest that IL-10 might modulate the downstream signal of TNF-α but not its expression in the setting of MCT-PAH. Overall, IL-10 affects the dynamics of cytokine networks involved in PA remodeling, and its site of action may differ according to the cytokine signal.

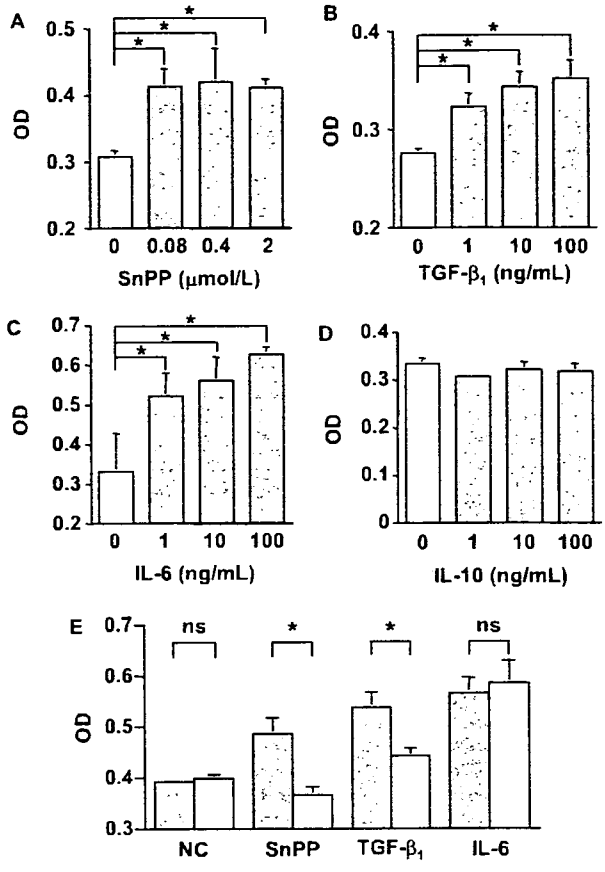

Figure 5. Antiproliferative effects of IL-10 on pulmonary arterial smooth muscle cells (PASMCs). The number of viable human PASMCs cultured in serum-free DMEM-F12 was estimated using a colorimetric assay (XTT assay). The optical density (OD) between 450 nm and 650 nm indicates the extent of cell proliferation. Addition of tin protoporphyrin IX (SnPP, A), TGF-β_1 (B), or IL-6 (C) dose-dependently promotes PASMC proliferation. Although IL-10 alone has no significant effect (D), pretreatment with IL-10 (10 ng/mL) inhibits PASMC proliferation induced by SnPP (2 μmol/L) or TGF-β_1 (20 ng/mL, E) but not that induced by IL-6 (20 ng/mL). Closed columns, cells not treated with IL-10; open columns, IL-10–treated cells. The results are representative of 3 independent experiments. Data represent mean±SEM ($n=4$ each, $^*P<0.05$). ns indicates not statistically significant.

CO induced by HO-1 blocks PASMC proliferation not only directly by inhibiting the expression of a cell cycle–specific transcription factor but also indirectly by attenuating mitogen signaling.[16] Interestingly, the transgenic mice that constitutively express HO-1 are protected from the development of hypoxia-induced PAH and excessive expression of a mitogen IL-6.[33] In this study, AAV-IL-10 administration increased the HO-1 level that negatively correlated with the IL-6 level in the lung of MCT-PAH rats. These observations suggest a dynamic relationship between IL-6 and HO-1 in PA remodeling progression. Chen et al[12] reported that AAV-IL-10 injection enhanced the activity and protein levels of HO-1, but SnPP treatment that inactivates HO-1 reversed the vasculoprotective effects of IL-10 in vivo. Here, we show that pretreatment with recombinant IL-10 suppressed the excessive PASMC proliferation induced by HO-1 inactivation with SnPP. Thus, IL-10 may sustain CO levels by maintaining

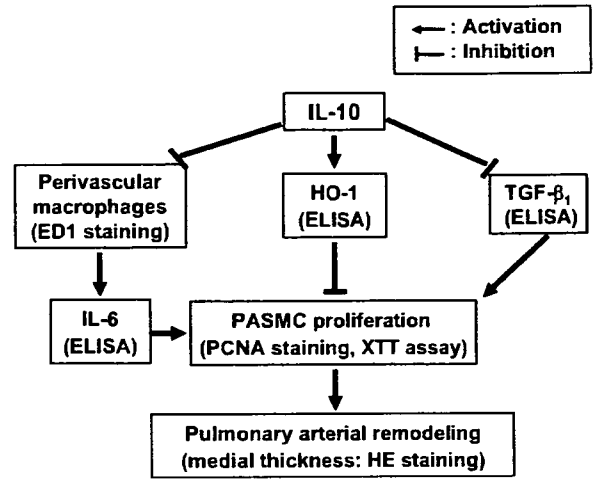

Figure 6. Proposed explanation for IL-10–mediated prevention of PAH and vascular remodeling. Monocrotaline treatment causes PAH in rats by inducing inflammation and proliferation of the PA. IL-10 prevents the development of PAH and PA remodeling by inhibiting vascular inflammation and proliferation. The effects of IL-10 are related to the decreased accumulation of perivascular macrophages and the reduced levels of active TGF-β_1 and IL-6. IL-10 induces HO-1 expression, which can negatively regulate inflammation and proliferation in the PA. IL-10 inhibits abnormal proliferation of PASMCs, thereby preventing PAH development.

HO-1 from inactivating, leading to the prevention of PA remodeling.

Finally, we will discuss the clinical implication and limitations of this study. Consistent with previous studies, maximum gene expression was noted 6 to 8 weeks after the intramuscular injection of AAV vectors. In this study, AAV-IL-10 was injected 4 weeks before MCT administration for the transgene expression to reach plateau levels when MCT-PAH was fully developed (3 to 4 weeks after the injection). Thus, our results are completely based on a prevention protocol, which may be rare in a clinical setting. Intramuscular AAV-IL-10 injection is an attractive candidate for antiinflammation therapy of PAH because inflammatory cytokine expression is associated with the clinical course of the disease. In addition, this strategy exhibited no life-threatening complications such as shock and sepsis which may occur in intravenous prostacyclin infusion therapy. However, therapeutic effects of IL-10 in established PAH has not been determined. Therefore, it should be further examined in studies using a treatment protocol. MCT-PAH is a widely-used and suitable model for exploring inflammatory mechanisms in PAH progression. However, how IL-10 affects other pathogenesis in PAH remains unknown. In the future, IL-10 function needs to be examined in other PAH models such as hypoxia-induced PAH.

In conclusion, AAV vector-mediated sustained IL-10 expression prevented the development of MCT-PAH in rats. The antiremodeling effects of IL-10 are related to the reduction of macrophage infiltration and pathological cytokine expression as well as increased HO-1 levels in the lung. Although the therapeutic role of IL-10 should be further investigated, our results provide new insights into molecular mechanisms underlying the development of human PAH.

Acknowledgments

We thank Miyoko Mitsu for her encouragement and technical support.

Sources of Funding

This work was supported by grants from (1) the Ministry of Health, Labor and Welfare of Japan; (2) Grants-in-Aid for Scientific Research; (3) grant for 21 Century COE Program; (4) "High-Tech Research Center" Project for Private Universities, matching fund subsidy, from the Ministry of Education, Culture, Sports, Science and Technology of Japan; and (5) The Research Award to Jichi Medical School Graduate Student.

Disclosures

None.

References

1. Humbert M, Sitbon O, Simonneau G. Treatment of pulmonary arterial hypertension. *N Engl J Med.* 2004;351:1425–1436.
2. Stenmark KR, Fagan KA, Frid MG. Hypoxia-induced pulmonary vascular remodeling: cellular and molecular mechanisms. *Circ Res.* 2006; 99:675–691.
3. Tuder RM, Groves B, Badesch DB, Voelkel NF. Exuberant endothelial cell growth and elements of inflammation are present in plexiform lesions of pulmonary hypertension. *Am J Pathol.* 1994;144:275–285.
4. Humbert M, Monti G, Brenot F, Sitbon O, Portier A, Grangeot-Keros L, Duroux P, Galanaud P, Simonneau G, Emilie D. Increased interleukin-1 and interleukin-6 serum concentrations in severe primary pulmonary hypertension. *Am J Respir Crit Care Med.* 1995;151:1628–1631.
5. Miyata M, Sakuma F, Yoshimura A, Ishikawa H, Nishimaki T, Kasukawa R. Pulmonary hypertension in rats. 2. Role of interleukin-6. *Int Arch Allergy Immunol.* 1995;108:287–291.
6. Miyata M, Sakuma F, Yoshimura A, Ishikawa H, Nishimaki T, Kasukawa R. Pulmonary hypertension in rats. 1. Role of bromodeoxyuridine-positive mononuclear cells and alveolar macrophages. *Int Arch Allergy Immunol.* 1995;108:281–286.
7. Arcot SS, Lipke DW, Gillespie MN, Olson JW. Alterations of growth factor transcripts in rat lungs during development of monocrotaline-induced pulmonary hypertension. *Biochem Pharmacol.* 1993;46: 1086–1091.
8. Karmochkine M, Wechsler B, Godeau P, Brenot F, Jagot JL, Simonneau G. Improvement of severe pulmonary hypertension in a patient with SLE. *Ann Rheum Dis.* 1996;55:561–562.
9. Bellotto F, Chiavacci P, Laveder F, Angelini A, Thiene G, Marcolongo R. Effective immunosuppressive therapy in a patient with primary pulmonary hypertension. *Thorax.* 1999;54:372–374.
10. Ito T, Ozawa K, Shimada K. Current drug targets and future therapy of pulmonary arterial hypertension. *Curr Med Chem.* 2007;14:719–733.
11. Ito T, Ikeda U. Inflammatory cytokines and cardiovascular disease. *Curr Drug Targets Inflamm Allergy.* 2003;2:257–265.
12. Chen S, Kapturczak MH, Wasserfall C, Glushakova OY, Campbell-Thompson M, Deshane JS, Joseph R, Cruz PE, Hauswirth WW, Madsen KM, Croker BP, Berns KI, Atkinson MA, Flotte TR, Tisher CC, Agarwal A. Interleukin 10 attenuates neointimal proliferation and inflammation in aortic allografts by a heme oxygenase-dependent pathway. *Proc Natl Acad Sci U S A.* 2005;102:7251–7256.
13. Mazighi M, Pelle A, Gonzalez W, Mtairag el M, Philippe M, Henin D, Michel JB, Feldman LJ. IL-10 inhibits vascular smooth muscle cell activation *in vitro* and *in vivo*. *Am J Physiol Heart Circ Physiol.* 2004; 287:H866–H871.
14. Yoshioka T, Okada T, Maeda Y, Ikeda U, Shimpo M, Nomoto T, Takeuchi K, Nonaka-Sarukawa M, Ito T, Takahashi M, Matsushita T, Mizukami H, Hanazono Y, Kume A, Ookawara S, Kawano M, Ishibashi S, Shimada K, Ozawa K. Adeno-associated virus vector-mediated interleukin-10 gene transfer inhibits atherosclerosis in apolipoprotein E-deficient mice. *Gene Ther.* 2004;11:1772–1779.
15. Li MC, He SH. IL-10 and its related cytokines for treatment of inflammatory bowel disease. *World J Gastroenterol.* 2004;10:620–625.
16. Morita T, Mitsialis SA, Koike H, Liu Y, Kourembanas S. Carbon monoxide controls the proliferation of hypoxic vascular smooth muscle cells. *J Biol Chem.* 1997;272:32804–32809.
17. Christou H, Morita T, Hsieh CM, Koike H, Arkonac B, Perrella MA, Kourembanas S. Prevention of hypoxia-induced pulmonary hypertension by enhancement of endogenous heme oxygenase-1 in the rat. *Circ Res.* 2000;86:1224–1229.
18. Yun S, Junbao D, Limin G, Chaomei Z, Xiuying T, Chaoshu T. The regulating effect of heme oxygenase/carbon monoxide on hypoxic pulmonary vascular structural remodeling. *Biochem Biophys Res Commun.* 2003;306:523–529.
19. Matsushita T, Elliger S, Elliger C, Podsakoff G, Villarreal L, Kurtzman GJ, Iwaki Y, Colosi P. Adeno-associated virus vectors can be efficiently produced without helper virus. *Gene Ther.* 1998;5:938–945.
20. Okada T, Nomoto T, Yoshioka T, Nonaka-Sarukawa M, Ito T, Ogura T, Iwata-Okada M, Uchibori R, Shimazaki K, Mizukami H, Kume A, Ozawa K. Large-scale production of recombinant viruses by use of a large culture vessel with active gassing. *Hum Gene Ther.* 2005;16:1212–1218.
21. Okada T, Nomoto T, Shimazaki K, Lijun W, Lu Y, Matsushita T, Mizukami H, Urabe M, Hanazono Y, Kume A, Muramatsu S, Nakano I, Ozawa K. Adeno-associated virus vectors for gene transfer to the brain. *Methods.* 2002;28:237–247.
22. Kay JM, Keane PM, Suyama KL, Gauthier D. Angiotensin converting enzyme activity and evolution of pulmonary vascular disease in rats with monocrotaline pulmonary hypertension. *Thorax.* 1982;37:88–96.
23. Yoshioka T, Ageyama N, Shibata H, Yasu T, Misawa Y, Takeuchi K, Matsui K, Yamamoto K, Terao K, Shimada K, Ikeda U, Ozawa K, Hanazono Y. Repair of infarcted myocardium mediated by transplanted bone marrow-derived CD34$^+$ stem cells in a nonhuman primate model. *Stem Cells.* 2005;23:355–364.
24. Lee TS, Chau LY. Heme oxygenase-1 mediates the anti-inflammatory effect of interleukin-10 in mice. *Nat Med.* 2002;8:240–246.
25. Voelkel NF, Tuder RM, Bridges J, Arend WP. Interleukin-1 receptor antagonist treatment reduces pulmonary hypertension generated in rats by monocrotaline. *Am J Respir Cell Mol Biol.* 1994;11:664–675.
26. Kimura H, Kasahara Y, Kurosu K, Sugito K, Takiguchi Y, Terai M, Mikata A, Natsume M, Mukaida N, Matsushima K, Kuriyama T. Alleviation of monocrotaline-induced pulmonary hypertension by antibodies to monocyte chemotactic and activating factor/monocyte chemoattractant protein-1. *Lab Invest.* 1998;78:571–581.
27. Selzman CH, McIntyre RC Jr, Shames BD, Whitehill TA, Banerjee A, Harken AH. Interleukin-10 inhibits human vascular smooth muscle proliferation. *J Mol Cell Cardiol.* 1998;30:889–896.
28. Morrell NW, Yang X, Upton PD, Jourdan KB, Morgan N, Sheares KK, Trembath RC. Altered growth responses of pulmonary artery smooth muscle cells from patients with primary pulmonary hypertension to transforming growth factor-β_1 and bone morphogenetic proteins. *Circulation.* 2001;104:790–795.
29. Botney MD, Bahadori L, Gold LI. Vascular remodeling in primary pulmonary hypertension. Potential role for transforming growth factor-β. *Am J Pathol.* 1994;144:286–295.
30. Tanaka Y, Schuster DP, Davis EC, Patterson GA, Botney MD. The role of vascular injury and hemodynamics in rat pulmonary artery remodeling. *J Clin Invest.* 1996;98:434–442.
31. El-Haroun H, Bradbury D, Clayton A, Knox AJ. Interleukin-1β, transforming growth factor-β_1, and bradykinin attenuate cyclic AMP production by human pulmonary artery smooth muscle cells in response to prostacyclin analogues and prostaglandin E2 by cyclooxygenase-2 induction and downregulation of adenylyl cyclase isoforms 1, 2, and 4. *Circ Res.* 2004;94:353–361.
32. Suzuki C, Takahashi M, Morimoto H, Izawa A, Ise H, Hongo M, Hoshikawa Y, Ito T, Miyashita H, Kobayashi E, Shimada K, Ikeda U. Mycophenolate mofetil attenuates pulmonary arterial hypertension in rats. *Biochem Biophys Res Commun.* 2006;349:781–788.
33. Minamino T, Christou H, Hsieh CM, Liu Y, Dhawan V, Abraham NG, Perrella MA, Mitsialis SA, Kourembanas S. Targeted expression of heme oxygenase-1 prevents the pulmonary inflammatory and vascular responses to hypoxia. *Proc Natl Acad Sci U S A.* 2001;98:8798–8803.

International Journal of
HEMATOLOGY

Relationship between the Binding Sites for von Willebrand Factor, Phospholipid, and Human Factor VIII C2 Inhibitor Alloantibodies within the Factor VIII C2 Domain

Keiji Nogami,[a] Midori Shima,[a] John C. Giddings,[b] Masahiro Takeyama,[a] Ichiro Tanaka,[a] Akira Yoshioka[a]

[a]Department of Pediatrics, Nara Medical University, Kashihara, Nara, Japan; [b]Department of Haematology, Wales College of Medicine, Cardiff University, UK

Received September 28, 2006; received in revised form January 12, 2007; accepted January 16, 2007

Abstract

Some factor VIII (FVIII) inhibitor alloantibodies block FVIII binding to von Willebrand factor (VWF) and phospholipid (PL) and recognize a C2 domain epitope that overlaps both binding sites. We previously showed that FVIII peptide 2315-2330 neutralized FVIII inhibitors and that Cys^{2326} and Glu^{2327} contributed to the maximum neutralizing effect. In the present study, we investigated the relationship between the essential binding sites for VWF, PL, and anti-C2 inhibitors by means of competitive-inhibition assays with overlapping synthetic peptides that span the C terminus of the C2 domain (residues 2288-2332). We identified 2 peptides (residues 2303-2317 and 2315-2330) that specifically blocked FVIII binding to VWF or PL by approximately 80% (50%-inhibitory concentration [IC_{50}], 9.0 μM) and 95% (IC_{50}, 0.12 μM), respectively. To examine in detail the residues responsible for PL binding, we prepared mutants of peptide 2315-2330 in which we sequentially substituted each residue with Gly. Two residues, Ile^{2317} and Met^{2321}, were shown to be essential for PL binding. Their substitution with Gly reduced the inhibitory effect by >90%. The data suggest that the binding sites for VWF, PL, and anti-C2 inhibitors in the C2 domain are in very close proximity but are not identical.

Int J Hematol. 2007;85:317-322. doi: 10.1532/IJH97.06192

Key words: Factor VIII; von Willebrand factor; Phospholipid; Binding; C2 domain; Inhibitors

1. Introduction

Factor VIII (FVIII), a plasma glycoprotein deficient or defective in individuals with the severe congenital bleeding disorder hemophilia A, functions as a cofactor in the tenase complex, which is responsible for the anionic phospholipid (PL) surface-dependent conversion of factor X to factor Xa by factor IXa [1]. FVIII is synthesized as a multidomain, single-chain molecule (A1-A2-B-A3-C1-C2) consisting of 2332 amino acid residues with a molecular mass of approximately 300 kd [2,3]. It is processed into a series of metal ion—dependent heterodimers by cleavage at the B-A3 junction, which generates a heavy chain (consisting of the A1 and A2 domains plus heterogeneous fragments of a partially proteolyzed B domain) that is linked to a light chain consisting of the A3, C1, and C2 domains [2-4].

Prior to thrombin- or factor Xa—catalyzed activation, FVIII circulates as a complex with von Willebrand factor (VWF), which protects and stabilizes FVIII [5,6]. Activation of FVIII by thrombin or factor Xa is associated with proteolytic cleavages at Arg^{372} and Arg^{740} in the heavy chain and at Arg^{1689} in the light chain [7]. The active form of FVIII (FVIIIa) is a heterotrimer consisting of the A1, A2, and A3-C1-C2 domains. FVIIIa dissociates from VWF and markedly enhances the catalytic efficiency of the tenase complex on the PL surface [8]. Thus, both VWF and PL govern the physiological function of FVIII.

Andersson and Brown [9] demonstrated that VWF interfered with FVIII binding to PL. Subsequently, investigators used preparations of recombinant C2 domain and anti-C2 monoclonal antibodies to show that VWF and PL bound directly to the C2 domain of FVIII [10,11]. Further studies using synthetic peptides in competitive-inhibition assays

Correspondence and reprint requests: Midori Shima, MD, PhD, Department of Pediatrics, Nara Medical University, 840 Shijo-cho, Kashihara City, Nara 634-8522, Japan; 81-744-29-8881; fax: 81-744-24-9222 (e-mail: mshima@naramed-u.ac.jp).

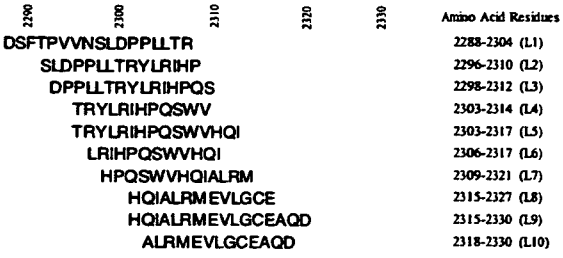

Figure 1. Schematic representation of the synthetic factor VIII (FVIII) peptides (L1-L10). The sequences of the FVIII peptides in the C terminus (residues 2288-2332) of the C2 domain are represented by their 1-letter abbreviations.

indicated that the C-terminal C2 region (residues 2303-2332) bound to VWF and PL [10,12]. All of these findings suggested that the sites of VWF and PL binding are in close proximity within the C2 domain.

The crystal structure of the C2 domain has been determined at an x-ray resolution of 1.5 Å [13]. A group of solvent-exposed hydrophobic "feet" consisting of Met^{2199}/Phe^{2220}, Val^{2223}, and Leu^{2251}/Leu^{2252}, and a ring of positively charged amino acid residues (Arg^{2215}, Arg^{2220}, Lys^{2227}, and Arg^{2320}) appear to be located behind the hydrophobic surface. These exposed hydrophobic residues in the C2 domain appear likely to contribute to PL binding [14].

FVIII inhibitors develop as alloantibodies in 20% to 30% of multitransfused patients with hemophilia A; they may also arise as autoantibodies in nonhemophilic individuals, resulting in acquired hemophilia A and a tendency for severe bleeding [15]. Inactivation of FVIII activity by these inhibitors is associated with impairment of FVIII cofactor function due to the binding of these antibodies to functionally or conformationally important epitopes in FVIII. Epitopes of this nature have been localized to one or more of the A2, C2, and A3-C1 domains [16-18]. In particular, anti-C2 inhibitors were found to prevent the interaction of FVIII with PL and VWF [11]. We previously demonstrated that C2 inhibitor epitopes, residues 2315-2330, were responsible for FVIII-neutralizing activity and that Cys^{2326} and Glu^{2327} were especially critical in this mechanism [19]. It appeared, therefore, that the epitopic region of anti-C2 inhibitors might overlap or juxtapose the binding site for VWF or PL in the C2 domain.

In the present study, we have more precisely localized the VWF- and PL-binding sites within the C2 domain and have investigated the relationship between the binding sites for VWF, PL, and anti-C2 inhibitors.

2. Materials and Methods

2.1. Reagents

Purified recombinant FVIII preparations were generous gifts from Bayer HealthCare (Berkeley, CA, USA). VWF was purified from plasma-derived FVIII/VWF concentrates (Confact F; The Chemo-Sero-Therapeutic Research Institute, Kumamoto, Japan) by gel filtration on a Sepharose CL-4B column (GE Healthcare, Uppsala, Sweden) and immunebeads coated with immobilized anti-FVIII monoclonal antibody, as has previously been reported [20]. An enzyme-linked immunosorbent assay (ELISA) did not detect FVIII antigen in the purified VWF preparation. JR8, a monoclonal antibody recognizing the A2 domain, was obtained from JR Scientific (Woodland, CA, USA). (α-Phosphatidyl-L-serine was purchased from Sigma-Aldrich (St. Louis, MO, USA). Synthetic peptides consisting of overlapping sequences of 12 to 17 residues corresponding to the C-terminal FVIII sequence (amino acid residues 2288-2332) were prepared by Bio-Synthesis (Lewisville, TX, USA) (Figure 1).

2.2. ELISA for the Binding of FVIII to Immobilized VWF or PL

Binding of FVIII to VWF or PL was examined as previously reported [11]. In brief, VWF (40 nM) or (α-phosphatidyl-L-serine (5 μM) was immobilized onto wells of microtiter plates. After blocking with 5% human serum albumin, FVIII (1 nM) was added to the immobilized VWF or PL. Bound FVIII was detected with a biotinylated anti-A2 monoclonal antibody (JR8) and horseradish peroxidase—labeled streptavidin. To determine the inhibitory effects of the synthetic peptides, we mixed various concentrations of peptides with FVIII prior to adding it to immobilized VWF or PL. The amount of nonspecific immunoglobulin G binding in the absence of FVIII was <5% of the total signal. Specific binding was estimated by subtracting the amount of nonspecific binding.

2.3. Hydropathy Analysis

The C-terminal end of the C2 domain (residues 2288-2332) was subjected to hydropathy analysis with the ProtScale program available from the ExPASy Web site (http://expasy.org/tools/protscale.html). In brief, the program performs a Kyte-Doolittle analysis with a moving 7-residue window that continuously determines the average hydropathy as the window is advanced through the sequence. Values that are more positive represent a greater probability of hydrophilicity and surface exposure.

3. Results

3.1. Effects of C2 Synthetic Peptides on FVIII Binding to VWF

Earlier studies reported that the C terminus of the C2 domain (residues 2303-2332) contained a VWF-binding site [10]. To further localize the VWF-binding site within this region, we used ELISA to examine the inhibitory effects of 10 overlapping synthetic peptides that encompass the C terminus of the C2 domain (residues 2288-2332) on FVIII binding to VWF (Figure 2). The L5 peptide (residues 2303-2317) blocked FVIII binding to VWF by approximately 80% at the maximum concentration employed (500 μM). This inhibition was dose dependent, and the 50%-inhibitory concentration (IC_{50}) was 9.0 ± 1.7 μM (mean ± SD). However, 2 peptides (L4, residues 2303-2314; L6, residues 2306-2317)

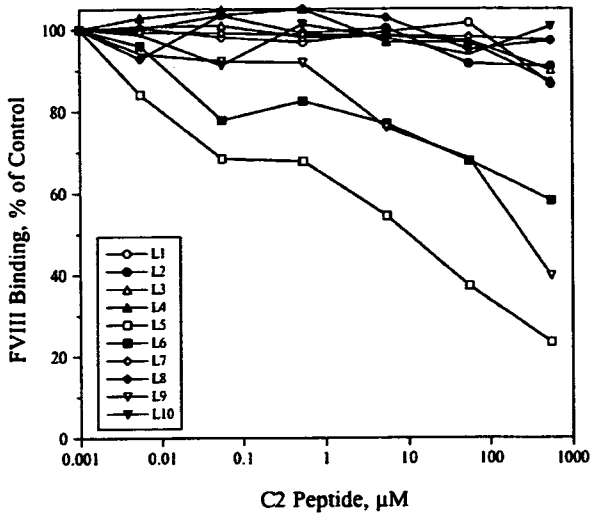

Figure 2. Effect of the C2 synthetic peptides on factor VIII (FVIII) binding to immobilized von Willebrand factor (VWF). FVIII (1 nM) was mixed with various concentrations of C2 synthetic peptide and then incubated with VWF (40 nM) immobilized onto wells of microtiter plates, as described in "Materials and Methods." Bound FVIII was detected with biotinylated anti-A2 immunoglobulin G (JR8). The absorbance values for FVIII binding to VWF in the absence of peptide represent the 100% level. The percentage of FVIII binding was plotted as a function of the C2 peptide concentration. Experiments were performed at least 3 separate times, and mean values are shown.

that had 3 residues removed from the C or the N terminus of the L5 peptide exhibited poor inhibition of this binding (approximately 10% and 40%, respectively). The L9 peptide (residues 2315-2330) also inhibited FVIII binding to VWF (by approximately 60%), but this effect was very weak, with an IC_{50} of approximately 250 μM. The other 6 peptides did not significantly inhibit binding. These data suggest that the 2303-2317 region in the C2 domain contained a VWF-interactive site.

3.2. Effects of C2 Synthetic Peptides on FVIII Binding to PL

Previous studies with synthetic peptides [12] demonstrated that the 2303-2332 region in the C terminus of the C2 domain inhibited FVIII binding to PL. To further localize the PL-interactive site within this region, we used ELISA to examine the inhibitory effects of these peptides on FVIII binding to PL (Figure 3). The L9 peptide completely blocked FVIII binding to PL at a concentration of 50 μM. This inhibition was dose dependent, and the IC_{50} value was 0.12 ± 0.02 μM. The L8 peptide (residues 2315-2327), in which 3 residues were removed from the C terminus of the L9 peptide, also completely blocked this binding in a dose-dependent manner, with an IC_{50} of 15 ± 4 μM. In contrast, the L10 peptide (residues 2318-2330), in which 3 residues were removed from the N terminus of the L9 peptide, poorly inhibited binding (approximately 45%), even at the maximum concentration. The L5 peptide, which inhibited FVIII and VWF interaction, also blocked FVIII binding to PL (by approximately 65%); however, the IC_{50} value (approximately 250 μM) was high compared with that obtained with VWF (approximately 9 μM). The other peptides did not significantly inhibit PL binding. These data suggest that the region of residues 2315 to 2330 in the C2 domain contains a PL-interactive site.

3.3. Hydropathy Analysis of the C terminus of the C2 Domain

To compare the properties of the interactive sites for VWF and PL in the C terminus of the C2 domain, we performed a hydropathy analysis of this region, as described in "Materials and Methods" (Figure 4). The results showed that the 2303-2317 sequence, which includes the VWF-interactive site, was hydrophilic and positioned on the exposed surface. In contrast, the 2315-2330 sequence, which includes the PL-interactive site, was hydrophobic and not exposed to the surface.

3.4. Effects of Individual Amino Acid Substitutions on the Ability of the L9 Peptide to Inhibit FVIII Binding to PL

Our previous findings showed that the L9 peptide (residues 2315-2330) neutralized the anti-FVIII activity of C2 inhibitor antibodies and that Cys^{2326} and Glu^{2327} in

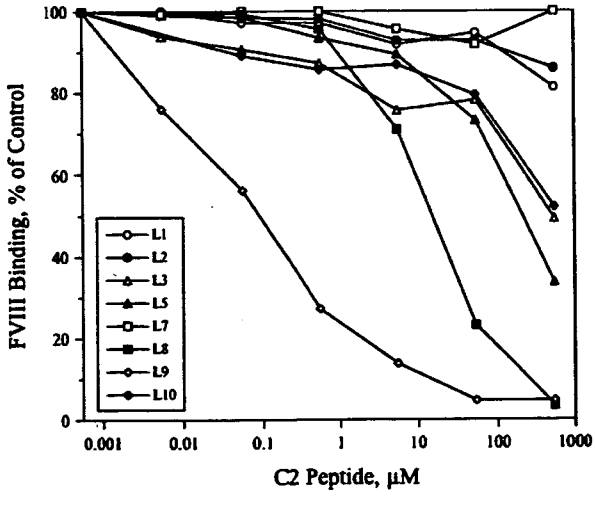

Figure 3. Effect of the C2 synthetic peptides on factor VIII (FVIII) binding to immobilized phospholipid (PL). FVIII (1 nM) was mixed with various concentrations of C2 synthetic peptides and then incubated with PL (5 μM) immobilized onto microtiter plate wells, as described in "Materials and Methods." Bound FVIII was detected with biotinylated anti-A2 immunoglobulin G (JR8). The absorbance values for FVIII binding to von Willebrand factor in the absence of peptide represent the 100% level. The percentage of FVIII binding was plotted as a function of the C2 peptide concentration. Experiments were performed at least 3 separate times, and mean values are shown.

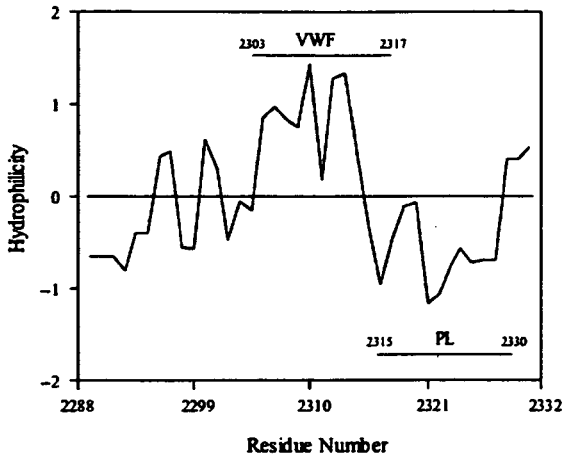

Figure 4. Hydropathy plot of the C terminus of the C2 domain. Residues 2288 to 2332 of the FVIII C2 domain were analyzed with the ProtScale program available from the ExPASy Web site (see "Materials and Methods"). A hydropathy scale from -2 (hydrophobic) to 2 (hydrophilic) was used to estimate the probability of a segment being exposed to the surface. The locations of the von Willebrand factor (VWF)- and phospholipid (PL)-binding regions obtained from the experiments with synthetic peptides are indicated by horizontal bars and residue numbers.

this sequence were required for the maximum effect [19]. Therefore, to compare the individual amino acid residues responsible for the inhibitory effect of the L9 peptide on FVIII and PL interaction, we prepared mutant peptides in which each residue in the 2315-2330 peptide (except for Gly^{2325}) was sequentially substituted with Gly. The ability of each mutant peptide (50 μM) to inhibit FVIII binding to PL was evaluated by ELISA (Figure 5). Substitution of Ile^{2317}, Leu^{2319}, Arg^{2320}, or Met^{2321} significantly reduced the capacity of the mutant peptide to inhibit FVIII binding to PL. The effect of substitution was most prominent when Ile^{2317} or Met^{2321} was replaced by Gly. In these instances, the inhibitory ability was reduced to <5%. Substitution of Leu^{2319} or Arg^{2320} reduced the inhibitory ability of the L9 peptide by approximately 40% and 50%, respectively. Increasing the concentrations of the mutant peptides to 500 μM did not affect their relative ability to inhibit FVIII binding to PL. These data suggest that the residues in the C terminus of the C2 domain responsible for PL binding are not identical to those responsible for binding of anti-C2 inhibitors.

4. Discussion

The C2 domain contains common antigenic determinants for most FVIII inhibitors. Furthermore, this domain contains the binding sites for VWF [10], PL [12], thrombin [21], and factor Xa [22]. In addition, our laboratory has demonstrated that binding of the metal ion Ca^{2+} to this domain supports the conformational structure of the light chain [23]. Thus, the C2 domain is essential for FVIII cofactor function and structure. Previous findings have also demonstrated that VWF, PL, and anti-C2 inhibitor antibodies compete for binding to the C2 domain [11], suggesting that their binding regions are in close proximity. Few reports have described their precise localizations, however. Using a panel of overlapping synthetic peptides, we previously localized the common C2 epitope for FVIII alloantibodies and monoclonal antibodies within 16 amino acid residues (2315-2330) in the C terminus of this domain [19]. We have now extended this study to examine the relationship between the VWF-binding site, the PL-binding site, and the C2 epitope.

Two major regions for VWF binding have been proposed on the basis of epitope analyses with monoclonal and polyclonal FVIII antibodies. One site appears to be located in the N-terminal highly acidic region of the A3 domain [24,25], and the other is in the C2 domain [9]. More recently, the C terminus of the A3 domain was also reported to be involved in the binding of VWF and activated protein C [26]. The precise mechanisms of these binding reactions remain unknown, however. Because the FVIII-neutralizing activity of FVIII alloantibodies with C2 epitopes was inhibited in the presence of VWF, it is possible that a region for

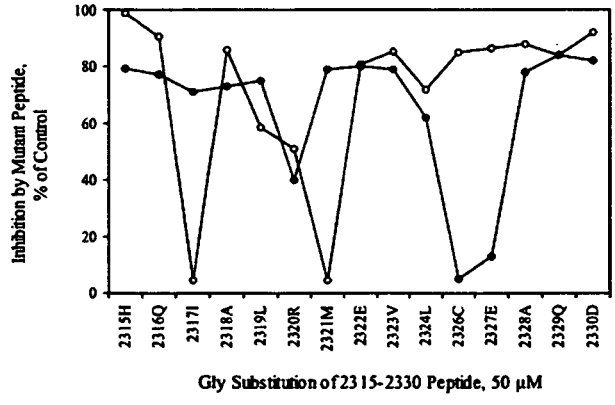

Figure 5. Effects of modified peptides on the ability of the L9 peptide to inhibit factor VIII (FVIII) binding to phospholipid (PL). Mutant L9 peptides were compared with the wild-type L9 peptide (control) for their ability to inhibit FVIII binding to PL (open circles). The horizontal axis shows the individual amino acid substituted in each mutant. The vertical axis shows the percentage of the control value: (percent inhibition of FVIII binding to PL by 50 μM mutant L9 peptide)/(percent inhibition of FVIII binding to PL by 50 μM wild-type L9 peptide) × 100. The control value for the wild-type L9 peptide was considered to be 100%. Experiments were performed at least 3 separate times, and mean values are shown. Previously published data (closed circles; see Figure 5 in [19]) are also shown to compare the effects of the substituted peptides on the ability of L9 to neutralize anti-FVIII antibody activity. The vertical axis shows the percentage of the control value: (percent residual FVIII activity in the presence of inhibitor antibody and 50 μM mutant L9 peptide)/(percent residual FVIII activity in the presence of inhibitor antibody and 50 μM wild-type L9 peptide) × 100. The mean values of 4 inhibitor antibodies are shown.

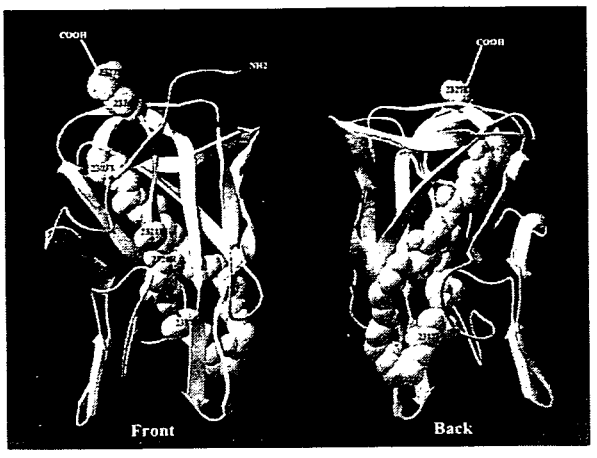

Figure 6. Binding epitopes for von Willebrand factor (VWF), phospholipid (PL), and anti-C2 inhibitor antibody on the factor VIII (FVIII) C2 domain. The FVIII C2 domain is shown in a ribbon format with β-sheets (yellow). The C2 residues responsible for VWF interaction (Thr^{2303}-Ile^{2317}) are shown in a space-filling format (green). The residues responsible for PL interaction (Ile^{2317}, Leu^{2319}, Arg^{2320}, and Met^{2321}) are shown in blue. The residues responsible for neutralizing the inhibitory activity of anti-C2 inhibitor antibody (Cys^{2326} and Glu^{2327}) are shown in pink.

VWF binding within the C2 domain is conformationally associated with the C2 epitope. Our binding experiments with overlapping synthetic peptides demonstrated that the L5 peptide (residues 2303-2317) inhibited FVIII binding to VWF (IC_{50}, 9 μM), suggesting that this region contained residues essential for VWF binding. Another 2 peptides, L4 (residues 2303-2314) and L6 (residues 2306-2317), in which the L5 peptide was truncated by 3 amino acid residues at the C terminus and the N terminus, respectively, failed to inhibit this binding (IC_{50}, >500 μM). Furthermore, peptides L2, L3, and L7, in which Thr-Arg-Tyr (residues 2303-2305) or His-Gln-Ile (residues 2315-2317) were deleted, did not inhibit this binding effectively. These data support the view that the interaction of VWF with the C terminus of the FVIII C2 domain requires conformationally stable 2303-2317 sequences. The inhibitory effect of the 2303-2317 peptide was not complete, however, suggesting the presence of an alternative VWF binding site. In this context, a reference to point mutations in the hemophilia A database and studies using mutagenesis [27] indicated that the C1-C2 marginal region containing Arg^{2150} is required for VWF binding. It seems likely, therefore, that both terminal portions of the C2 domain are juxtaposed spatially, that this juxtaposition is mediated by a disulfide bond between Cys^{2174} and Cys^{2326} [13,28], and that VWF binds to distinct sites in both terminal portions of the C2 domain.

The association of FVIII and VWF is based on a noncovalent electrostatic interaction. Hence, FVIII is readily dissociated from VWF at high cation concentrations [29]. Hydropathy analysis showed that the peptide region of VWF binding contains hydrophilic residues, and considering that the N-terminal A3 domain also contains highly acidic amino acid residues [24,25], VWF binding may require hydrophilic residues exposed on the surface of the FVIII molecule. The association of FVIII and VWF is restricted in the presence of PL [9], and the assembly of the tenase complex on membrane surfaces is enhanced in these circumstances. Foster et al [12] previously demonstrated that a peptide corresponding to residues 2303 to 2332 competes with FVIII for binding to PL. In our studies, the L9 peptide (residues 2315-2330) inhibited FVIII binding to PL (IC_{50}, 0.12 μM), confirming that this region contains a PL-binding site. Similarly, the L10 peptide (residues 2318-2330) completely inhibited PL binding, although the IC_{50} value was higher (15 μM). In addition, the L5 peptide (residues 2303-2317), which inhibited VWF binding, also weakly inhibited PL binding (IC_{50}, approximately 250 μM). In contrast, the L8 peptide (residues 2315-2327) failed to inhibit PL binding (IC_{50}, >500 μM). These data suggested that residues 2315 to 2317 (His-Gln-Ile) contributed significantly to PL interactions. Furthermore, the studies with mutant peptides in which individual amino acids were substituted with Gly revealed that Ile^{2317}, Leu^{2319}, Arg^{2320}, and Met^{2321} in the C terminus of the C2 domain were closely associated with PL binding.

The crystal structure of the C2 domain has been shown to consist of a β-sandwich core with 2 β-sheet turns and an adjacent loop, which display a group of solvent-exposed hydrophobic "feet" consisting of Met^{2199}/Phe^{2220}, Val^{2223}, and Leu^{2251}/Leu^{2252} [13]. A ring of positively charged amino acid residues (Arg^{2215}, Arg^{2220}, Lys^{2227}, and Arg^{2320}) was located behind the hydrophobic surface. These exposed hydrophobic and surrounding positively charged residues appeared likely to contribute to membrane binding. Our current data are in keeping with these proposals and suggest that Arg^{2320} and the surrounding residues (Ile^{2317}, Leu^{2319}, and Met^{2321}) located in the C-terminal portion of the C2 domain are essential for PL binding. Our data further indicate that the VWF-binding site and the PL-binding site are in very close proximity in the C2 domain but are not identical. Interestingly, the binding sites for VWF and PL are hydrophilic and hydrophobic, respectively, and comparisons of the amino acid sequences for human, porcine, murine, and canine FVIII molecules (http://europium.csc.mrc.ac.uk) indicate that the residues of both the 2303-2317 and 2315-2330 sequences are well conserved.

In summary, we have successfully identified precise regions of PL and VWF binding within the C2 domain of FVIII. Given the crystal structure of the C2 domain [13], the results of our peptide experiments demonstrate that the binding sites for PL, VWF, and anti-C2 inhibitors are in very close proximity (Figure 6). The results of competitive-inhibition studies can be explained by this close relationship within the C-terminal portion of the C2 domain.

Acknowledgments

This work was partly supported by grants for MEXT KAKENHI (17390304 and 17591110) and for AIDS Research from the Ministry of Health, Labor and Welfare of Japan.

References

1. Mann KG, Nesheim ME, Church WR, Haley P, Krishnaswamy S. Surface-dependent reactions of the vitamin K-dependent enzyme complexes. *Blood*. 1990;76:1-16.
2. Wood WI, Capon DJ, Simonsen CC, et al. Expression of active human factor VIII from recombinant DNA clones. *Nature*. 1984;312:330-337.
3. Vehar GA, Keyt B, Eaton D, et al. Structure of human factor VIII. *Nature*. 1984;312:337-342.
4. Fay PJ, Anderson MT, Chavin SI, Marder VJ. The size of human factor VIII heterodimers and the effects produced by thrombin. *Biochim Biophys Acta*. 1986;871:268-278.
5. Weiss HJ, Sussman II, Hoyer LW. Stabilization of factor VIII in plasma by the von Willebrand factor: studies on posttransfusion and dissociated factor VIII and in patients with von Willebrand's disease. *J Clin Invest*. 1977;60:390-404.
6. Hoyer LW. The factor VIII complex: structure and function. *Blood*. 1981;58:1-13.
7. Eaton D, Rodriguez H, Vehar GA. Proteolytic processing of human factor VIII: correlation of specific cleavages by thrombin, factor Xa, and activated protein C with activation and inactivation of factor VIII coagulant activity. *Biochemistry*. 1986;25:505-512.
8. van Dieijen G, Tans G, Rosing J, Hemker HC. The role of phospholipid and factor VIIIa in the activation of bovine factor X *J Biol Chem*. 1981;256:3433-3442.
9. Andersson LO, Brown JE. Interaction of factor VIII-von Willebrand factor with phospholipid vesicles. *Biochem J*. 1981;200:161-167.
10. Saenko EL, Shima M, Rajalakshmi KJ, Scandella D. A role for the C2 domain of factor VIII in binding to von Willebrand factor. *J Biol Chem*. 1994;269:11601-11605.
11. Shima M, Scandella D, Yoshioka A, et al. A factor VIII neutralizing monoclonal antibody and a human inhibitor alloantibody recognizing epitopes in the C2 domain inhibit factor VIII binding to von Willebrand factor and to phosphatidylserine. *Thromb Haemost*. 1993;69:240-246.
12. Foster PA, Fulcher CA, Houghten RA, Zimmerman TS. Synthetic factor VIII peptides with amino acid sequences contained within the C2 domain of factor VIII inhibit factor VIII binding to phosphatidylserine. *Blood*. 1990;75:1999-2004.
13. Pratt KP, Shen BW, Takeshima K, Davie EW, Fujikawa K, Stoddard BL. Structure of the C2 domain of human factor VIII at 1.5 Å resolution. *Nature*. 1999;402:439-442.
14. Barrow RT, Healey JF, Jacquemin MG, Saint-Remy JM, Lollar P. Antigenicity of putative phospholipid membrane-binding residues in factor VIII. *Blood*. 2001;97:169-174.
15. Gill FM. The natural history of factor VIII inhibitors in patients with hemophilia A. In: Hoyer LW, ed. *Factor VIII Inhibitors*. New York, NY: Alan R Liss; 1984:19-28.
16. Healey JF, Lubin IM, Nakai H, et al. Residues 484-508 contain a major determinant of the inhibitory epitope in the A2 domain of human factor VIII. *J Biol Chem*. 1995;270:14505-14509.
17. Scandella D, Mattingly M, de Graaf S, Fulcher CA. Localization of epitopes for human factor VIII inhibitor antibodies by immunoblotting and antibody neutralization. *Blood*. 1989;74: 1618-1626.
18. Zhong D, Saenko EL, Shima M, Felch M, Scandella D. Some human inhibitor antibodies interfere with factor VIII binding to factor IX. *Blood*. 1998;92:136-142.
19. Nogami K, Shima M, Nakai H, et al. Identification of a factor VIII peptide, residues 2315-2330, which neutralizes human factor VIII C2 inhibitor alloantibodies: requirement of Cys^{2326} and Glu^{2327} for maximum effect. *Br J Haematol*. 1999;107:196-203.
20. Shima M, Yoshioka A, Nakajima M, Nakai H, Fukui H. A monoclonal antibody (NMC-VIII/10) to factor VIII light chain recognizing Glu1675-Glu1684 inhibits factor VIII binding to endogenous von Willebrand factor in human umbilical vein endothelial cells. *Br J Haematol*. 1992;81:533-538.
21. Nogami K, Shima M, Hosokawa K, et al. Factor VIII C2 domain contains the thrombin-binding site responsible for thrombin-catalyzed cleavage at Arg^{1689}. *J Biol Chem*. 2000;275:25774-25780.
22. Nogami K, Shima M, Hosokawa K, et al. Role of factor VIII C2 domain in factor VIII binding to factor Xa. *J Biol Chem*. 1999;274:31000-31007.
23. Takeyama M, Nogami K, Okuda M, et al. von Willebrand factor protects Ca^{2+}-dependent structure of the factor VIII light chain [abstract]. *Blood*. 2005;106:295a.
24. Foster PA, Fulcher CA, Houghten RA, Zimmerman TS. An immunogenic region within residues Val^{1670}-Glu^{1684} of the factor VIII light chain induces antibodies which inhibit binding of factor VIII to von Willebrand factor. *J Biol Chem*. 1988;263: 5230-5234.
25. Shima M, Yoshioka A, Nakai H, et al. Epitope localization of monoclonal antibodies against factor VIII light chain which inhibit complex formation by factor VIII with von Willebrand factor. *Int J Hematol*. 1991;54:515-522.
26. Nogami K, Shima M, Nishiya K, et al. A novel mechanism of factor VIII protection by von Willebrand factor from activated protein C-catalyzed inactivation. *Blood*. 2002;99:3993-3998.
27. Jacquemin M, Benhida A, Peerlinck K, et al. A human antibody directed to the factor VIII C1 domain inhibits factor VIII cofactor activity and binding to von Willebrand factor. *Blood*. 2000;95: 156-163.
28. McMullen BA, Fujikawa K, Davie EW, Hedner U, Ezban M. Locations of disulfide bonds and free cysteines in the heavy and light chains of recombinant human factor VIII (antihemophilic factor A). *Protein Sci*. 1995;4:740-746.
29. Hamer RJ, Koedam JA, Beeser-Visser NH, Sixma JJ. The effect of thrombin on the complex between factor VIII and von Willebrand factor. *Eur J Biochem*. 1987;167:253-259.

International Journal of
HEMATOLOGY

Factor VIII–Mediated Global Hemostasis in the Absence of von Willebrand Factor

Masahiro Takeyama, Shogo Kasuda, Yoshihiko Sakurai, Midori Shima, Tomohiro Takeda, Shoko Omura, Hiroyuki Naka, Akira Yoshioka

Department of Pediatrics, Nara Medical University School of Medicine, Kashihara, Japan

Received November 15, 2006; received in revised form January 24, 2007; accepted February 14, 2007

Abstract

Although the efficacy of recombinant factor VIII (rFVIII) in the treatment of type 3 von Willebrand disease (VWD) has been reported, the mechanisms by which FVIII concentrates devoid of von Willebrand factor (VWF) induce improvements in hemostasis are poorly understood. To address the role of FVIII or intrinsic coagulation in the absence of VWF, we performed a hemostatic analysis. Blood samples were obtained before and after the administration of rFVIII to 2 patients with type 3 VWD. A rotating thromboelastometry assay was performed to examine global interactions in hemostasis. Studies of thrombin- and shear-induced platelet aggregation were also conducted to elucidate the effect on platelet activation. Furthermore, we assessed the rise in the thrombin-induced intracellular concentration of free calcium ($[Ca^{2+}]_i$). Addition of rFVIII to preinfusion blood in vitro corrected thromboelastometric parameters and thrombin-induced aggregation. In ex vivo studies, thromboelastometry analysis showed that rFVIII shortened the onset and progression of the coagulation process. Furthermore, rFVIII corrected low shear–induced and thrombin-induced platelet aggregation in platelet-rich plasma. In addition, rFVIII improved thrombin-induced $[Ca^{2+}]_i$ flux in washed platelets. Our observations suggested that FVIII is incorporated into platelets to activate them, as well as to act directly in intrinsic coagulation in the absence of VWF. FVIII may play a critical role even in the absence of VWF.

Int J Hematol. 2007;85:397-402. doi: 10.1532/IJH97.06214

Key words: Factor VIII; Intrinsic coagulation; von Willebrand disease; Calcium; Platelet activation

1. Introduction

von Willebrand factor (VWF) mediates the adhesion of platelets to damaged vascular walls and serves as a carrier for intrinsic coagulation factor VIII (FVIII) to protect this molecule from plasma proteinases. Thus, a deficiency of VWF results in defective platelet deposition on the subendothelial matrix, as well as a shortened FVIII half-life and very low levels of circulating FVIII. In the absence of VWF, such as in type 3 von Willebrand disease (VWD) (complete deficiency of VWF [1]), the usually severe hemostatic defect can lead to abnormal hemorrhage similar to that seen in patients with hemophilia A.

Because a recent cell-based model described the close links between coagulation and thrombin-mediated platelet activation [2], we hypothesized that when the coagulation system is sufficiently evoked, normal hemostasis, including both secondary and primary hemostasis, would occur even in the absence of VWF. In fact, FVIII concentrates devoid of VWF have been successfully used for the treatment of type 3 VWD patients, with or without VWF-neutralizing alloantibodies (inhibitors) [3-6]. These observations seem to provide clinical support for our hypothesis, but the detailed mechanism by which FVIII devoid of VWF exerts a hemostatic effect (and specifically its effects on platelets) remains to be elucidated. To test the hypothesis, we investigated the hemostatic effects of FVIII on type 3 VWD plasma by using rotation thromboelastometry (ROTEM), platelet-aggregation studies, and measurements of the intracellular concentration of free calcium ($[Ca^{2+}]_i$).

M.T. and S.K. contributed equally to this work.

Present address for S.K.: Department of Legal Medicine, Hyogo College of Medicine, Nishinomiya, Japan.

Correspondence and reprint requests: Midori Shima, MD, PhD, Department of Pediatrics, Nara Medical University School of Medicine, 840, Shijyo-cho, Kashihara, Nara 634-8522, Japan; 81-744-29-8881; fax: 81-744-24-9222 (e-mail: mshima@naramed-u.ac.jp).

2. Materials and Methods

2.1. Materials

Recombinant FVIII (rFVIII) (Kogenate® FS) was kindly donated by Bayer Yakuhin (Osaka, Japan). Ristocetin and α-thrombin were purchased from Sigma-Aldrich (St. Louis, MO, USA). All other reagents were purchased from Wako Pure Chemical Industries (Osaka, Japan).

2.2. Patients

The patients were a 4-year-old boy (patient 1) and a 55-year-old man (patient 2) with type 3 VWD. Neither patient showed the presence of VWF antigen by enzyme-linked immunosorbent assay or multimer analysis. The patients' FVIII coagulant activities (FVIII:C) were 2.0% and 1.0%, respectively. Blood samples were obtained before injection, at 30 minutes after bolus injection (50 U/kg), and, in some experiments, at 6 hours after continuous infusion (5 U/kg per hour) of rFVIII for oral bleeding (patient 1) and the extraction of multiple teeth (patient 2). The FVIII:C is considered to reach a steady state 6 hours after continuous infusion. The half-life of FVIII is shortened in type 3 VWD because of the lack of the protective effect of VWF. Mathematical modeling of FVIII kinetics revealed that the half-life of FVIII is 37 - minutes in the absence of VWF [7]. Actually, in both patients in this study, the FVIII:C level was increased up to approximately 30% after bolus injection and to approximately 10% during continuous infusion. Lower than expected levels of FVIII:C at 30 minutes after bolus infusion suggested that the half-life of FVIII in vivo is shorter than the calculated half-life. Therefore, the effects of continuous infusion can be assessed 6 hours after continuous infusion without having to consider the effect of FVIII administered initially by bolus injection. The clinical course of patient 2 has been described elsewhere [6].

2.3. Blood and Platelet Preparation

Informed and written consent was obtained from 3 healthy volunteers who had not taken medication for at least 2 weeks, from patient 2, and from the guardians of patient 1. The samples were anticoagulated with 3.8% sodium citrate (9:1, vol/vol). Platelet-rich plasma (PRP) was prepared by centrifugation at 200*g* for 10 minutes. Platelet-poor plasma was obtained after further centrifugation at 1500*g* for 20 minutes. This study was approved by the ethics committee of Nara Medical University.

2.4. Rotation Thromboelastometry

To obtain good reproducibility, we carried out ROTEM (ROTEM Whole Blood Haemostasis Analyzer; Pentapharm, Munich, Germany) with whole blood that had been stored at room temperature for 30 minutes following blood collection [8]. In the ex vivo study, we commenced analysis when 300 μL of blood was recalcified with 20 μL of 0.2 M $CaCl_2$. To assess the effects of rFVIII on ROTEM parameters in vitro, we mixed 20 μL of various concentrations of rFVIII with 280 μL of citrated whole blood from a patient with type 3 VWD and incubated the blood at 37°C for 5 minutes. We measured several parameters. Clotting time (CT) was defined as the time from the starting point to initial fibrin formation, as determined by a signal amplitude of 2 mm. This parameter is similar to the whole blood CT. The clot-formation time (CFT), defined as the time from the CT end point until the signal amplitude reached 20 mm, is a measure of the speed at which a clot forms with a given viscoelastic strength. The α angle was measured between the midline of the tracing and a line drawn from the 1-mm point tangential to the curve. The α value and the CFT indicate the rate of increase of the elastic shear modulus in the sample. Maximum clot firmness (MCF) was noted as the largest amplitude of the thromboelastometric signal and is a measure of clot strength. The velocity of clot formation was analyzed with ROTEM Systems software (Pentapharm).

2.5. Agonist- and Shear-Induced Platelet Aggregation in PRP

Platelet aggregation in PRP was monitored by the light-transmittance method with an optical aggregometer (Hematracer 1; NKK, Tokyo, Japan). To assess the effects of rFVIII on platelet aggregation in vitro, we mixed 80 μL of various concentrations of rFVIII with 160 μL of type 3 VWD PRP and incubated the plasma at 37°C for 5 minutes. Aggregation was induced by the addition of collagen, α-thrombin, and ristocetin. The concentrations of these agonists were adjusted such that submaximal aggregation (approximately 80% of total aggregation in normal PRP) was achieved in the collagen- and the ristocetin-induced platelet-aggregation studies, thereby allowing the quantification of any enhancement of platelet aggregation [9]. The lowest concentration at which secondary aggregation occurred in normal platelets was used for α-thrombin so that early fibrin formation did not mask platelet aggregation.

Shear-induced platelet aggregation (SIPA) was measured with a modified cone-plate viscometer [10] with citrated PRP under constant low shear (12 dyne/cm^2 [L-SIPA]) and high shear (108 dyne/cm^2 [H-SIPA]) [11]. To assess the effects of rFVIII on SIPA in vitro, we mixed 100 μL of various rFVIII concentrations with 300 μL of type 3 VWD PRP and incubated the plasma at 37°C for 5 minutes. All aggregation studies were performed in duplicate or triplicate at a final platelet count of 300 × 10^6/mL.

2.6. Thrombin-Induced Increase in the $[Ca^{2+}]_i$ of Platelets

Platelets from anticoagulated PRP were washed and loaded with fura-2 AM according to the method described by Pollock and Rink [12]. After stimulation with α-thrombin at 2 concentrations (0.5 nM and 10 nM), changes in $[Ca^{2+}]_i$ were measured in duplicate with a fluorescence spectrophotometer (CAF110 system; Jasco, Tokyo, Japan), and the $[Ca^{2+}]_i$ was calculated as previously described [13,14].

2.7. Statistical Analysis

Results were expressed as the mean or the mean ± SE. The paired Student *t* test was used for comparisons of

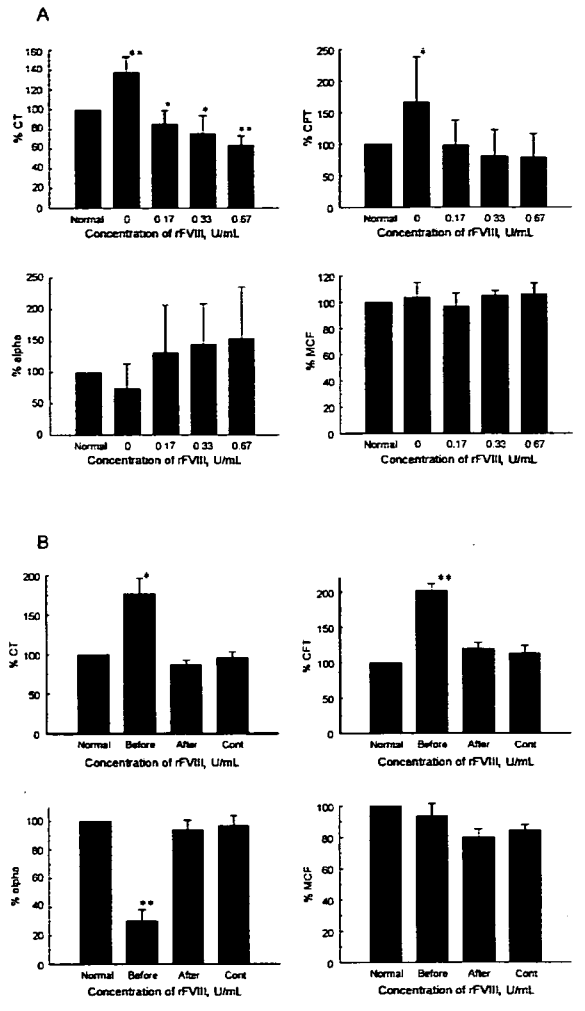

Figure 1. Effect of factor VIII (FVIII) on rotation thromboelastometry (ROTEM) parameters, clotting time (CT), clot-formation time (CFT), and maximum clot firmness (MCF). A, The effects of recombinant FVIII (rFVIII) on ROTEM parameters in vitro were assessed in the presence and absence of rFVIII (final concentrations: 0, 0.17, 0.33, and 0.67 U/mL). Addition of rFVIII significantly accelerated the CT and CFT and increased α but not the MCF. Data are presented as percentages of the control response (healthy subject) (n = 6, 3 from patient 1 and 3 from patient 2. $*P < .05$; $**P < .01$. B, The effect of rFVIII on ROTEM parameters ex vivo was assessed with patient plasma obtained before and after bolus infusion and during continuous infusion (Cont). After intravenous administration of rFVIII, the CT, CFT, and α were normalized, and the MCF was reduced. Data are presented as percentages of the control response (healthy subject) (n = 6, 3 from patient 1 and 3 from patient 2). $*P < .05$; $**P < .01$.

repeated measurements. Multiple groups were compared with 1-way analysis of variance and the Student-Newman-Keuls test.

3. Results

3.1. Effects of rFVIII on ROTEM Parameters

ROTEM parameters were measured to evaluate overall interactions in hemostasis. Addition of rFVIII in vitro (final concentration, 0.17 U/mL) to whole blood from 2 patients with type 3 VWD produced thromboelastometric changes, including a significant reduction in the CT, a concurrent reduction in the CFT, an increase in α (Figure 1A), and an increase in the velocity of clot formation (Figure 2A). These changes were dose dependent and statistically significant. The rFVIII concentration of 0.17 U/mL in whole blood was comparable to a circulating level of approximately 40% of the FVIII:C at a hematocrit of 43% to 45% in these 2 patients. These in vitro results indicated that the addition of rFVIII supported procoagulant activity and increased the rate of the shear modulus.

Similarly, intravenous administration of rFVIII in both patients with type 3 VWD significantly decreased the CT and CFT and increased α and the velocity of clot formation. The MCF appeared to decrease in these ex vivo studies, but the change was not statistically significant (Figures 1B and 2B).

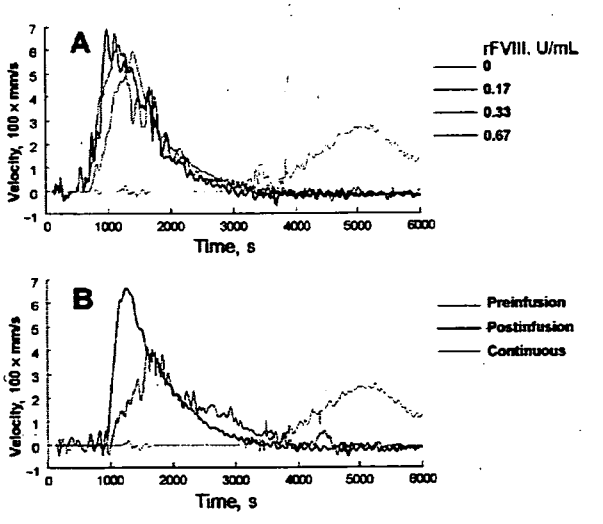

Figure 2. Effect of recombinant factor VIII (rFVIII) infusion on the rotation thromboelastometry (ROTEM) velocity of clot formation. A, The effect of rFVIII on the ROTEM velocity of clot formation in vitro was assessed in the presence and absence of rFVIII (final concentrations: 0, 0.17, 0.33, and 0.67 U/mL). Addition of rFVIII increased the velocity of clot formation and reduced the time to maximum velocity in a dose-dependent manner. The results shown here are representative of experiments using blood from patient 1. B, The effect of rFVIII on the ROTEM velocity ex vivo was assessed with plasma obtained before (Preinfusion) and after (Postinfusion) bolus infusion and during continuous infusion (Continuous). After intravenous rFVIII administration, the velocity increased, and the maximum velocity time was reduced. The results shown here are representative of experiments using blood from patient 2. Experiments were repeated twice, each time with whole blood from the 2 patients, with similar results.

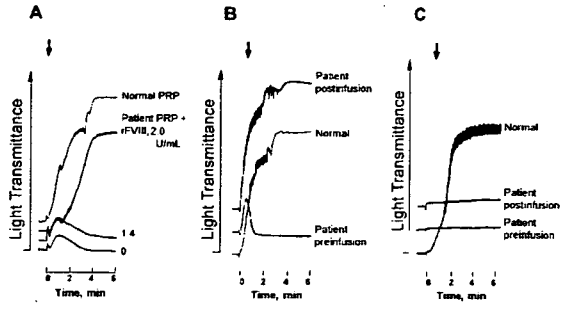

Figure 3. Effect of recombinant factor VIII (rFVIII) on α-thrombin–induced platelet aggregation. A, Effect of rFVIII on thrombin-induced platelet aggregation in vitro. Platelet-rich plasma (PRP) from the patient was preincubated for 5 minutes in the presence or absence of rFVIII (final concentrations: 0, 1.4, and 2.0 U/mL) before the addition of thrombin. B, Effect of rFVIII infusion on thrombin-induced platelet aggregation ex vivo. Aggregation of normal PRP (Normal), patient PRP before rFVIII infusion (preinfusion), and patient PRP 30 minutes after infusion (postinfusion). C, Effect of rFVIII infusion on ristocetin-induced platelet aggregation ex vivo. Ristocetin-induced aggregation of normal PRP (Normal), patient PRP before rFVIII infusion (preinfusion), and patient PRP 30 minutes after infusion (postinfusion). The platelet count was adjusted to 300×10^6/mL. Experiments were repeated 3 or 4 times with PRP from each of the 2 patients, with similar results. The results shown here are from the experiments with blood from patient 2. Arrows indicate the addition of α-thrombin or ristocetin.

3.2. Effects of rFVIII on Agonist-Induced Platelet Aggregation in PRP

Studies of agonist-induced platelet aggregation were performed with blood from patients with type 3 VWD to determine how the presence of rFVIII affected platelet function. Submaximal aggregation conditions were adopted to assess the difference between type 3 VWD PRP with and without rFVIII as well as the difference before and after rFVIII-replacement therapy. The type 3 VWD native PRP responded well to collagen and was slightly affected by the addition of rFVIII (data not shown). In thrombin-induced aggregation in vitro, however, a weak response was seen in native PRP, and this response was enhanced by rFVIII addition, although a final rFVIII concentration of 2.0 U/mL was required to mediate maximum aggregation (Figure 3A). There was a slight response of the type 3 VWD platelets to ristocetin both before and after the addition of rFVIII (data not shown).

PRP from the patients with type 3 VWD was used to examine thrombin- and ristocetin-induced platelet aggregation ex vivo before and after rFVIII infusion. rFVIII replacement potentiated thrombin-induced platelet aggregation to an extent comparable with normal aggregation (percent maximal aggregation, 26.3% before infusion versus 98.2% after infusion; normal, 100% [Figure 3B]) but did not improve ristocetin-induced platelet aggregation (Figure 3C).

3.3. Effects of rFVIII on SIPA

In vitro addition of rFVIII to type 3 VWD PRP had little effect on curves of shear-induced aggregation. Almost no aggregation was seen under high-shear conditions, and only slight aggregation was observed under low-shear conditions, both in the presence and absence of rFVIII (data not shown). In contrast, aggregation induced by low shear was significantly improved after rFVIII infusion (Figure 4A), whereas minute platelet aggregation was observed under high-shear conditions ex vivo, both before and after rFVIII replacement (Figure 4B).

3.4. Effects of rFVIII on Calcium Flux in Thrombin-Induced Platelet Aggregation

We assessed thrombin-induced cytoplasmic Ca^{2+} mobilization ex vivo to examine more precisely the effects of FVIII on platelet function. Figure 5 shows typical traces of fluorescence and optical density of fura-2–loaded platelets from patients with type 3 VWD that had been activated by 0.5 nM and 10 nM α-thrombin before and after rFVIII replacement. An increase in both maximum washed-platelet aggregation and $[Ca^{2+}]_i$ was observed at both thrombin concentrations.

4. Discussion

We have shown by in vitro and ex vivo experiments that the hemostatic mechanism including platelet activation is supported by FVIII, even in the absence of VWF. Increased levels of FVIII in the absence of VWF improved (1) ROTEM parameter values in vitro and ex vivo, (2) the responsiveness of platelets to thrombin in vitro and ex vivo, (3) the response to L-SIPA ex vivo, and (4) ex vivo thrombin-induced mobilization of platelet $[Ca^{2+}]_i$.

ROTEM provides an overall measure of interactions during hemostasis, reflecting the coagulation cascade, the fibrinogen level, and platelet activation [15]. In the present studies, rFVIII devoid of VWF corrected the values of all ROTEM parameters (with the exception of MCF) both in

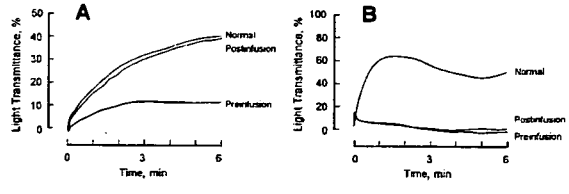

Figure 4. Effect of recombinant factor VIII (rFVIII) infusion on shear-induced platelet aggregation. Normal or patient platelet-rich plasma (PRP) was exposed to low shear stress (12 dyne/cm^2) (A) or high shear stress (108 dyne/cm^2) (B) for 6 minutes by means of a modified cone-plate viscometer. Results are for normal PRP (Normal) and patient plasma obtained before (Preinfusion) and after (Postinfusion) bolus infusion. The platelet count was adjusted to 300×10^6/mL. Experiments were repeated 2 or 3 times with PRP from each of 2 patients with type 3 VWD, with similar results. The results shown are from the experiments with patient 1 PRP.

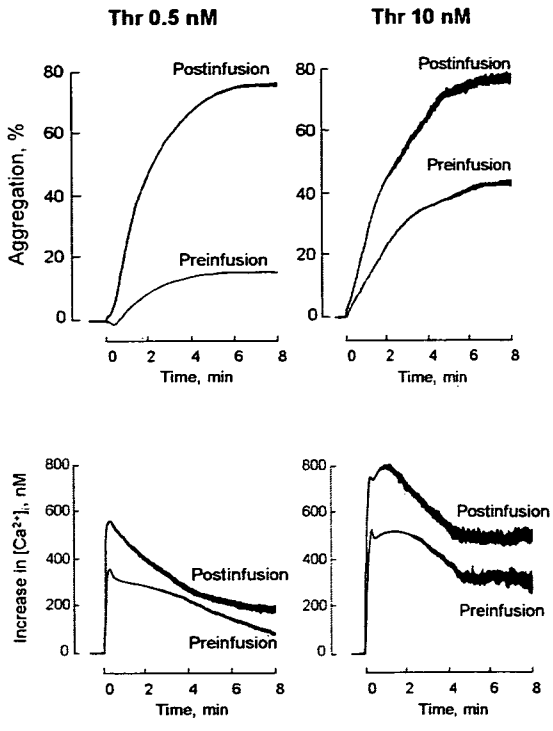

Figure 5. Effect of recombinant factor VIII (rFVIII) on the α-thrombin–induced flux of the intracellular concentration of free calcium ($[Ca^{2+}]_i$) (bottom) and the aggregation of washed platelets (top). Low (0.5 nM) and high (10 nM) concentrations of α-thrombin (Thr) were used to assess the effect of rFVIII on protease-activated receptors. The platelet count was adjusted to 300 x 10^6/mL. Results are for patient plasma obtained before (Preinfusion) and after (Postinfusion) bolus infusion of FVIII. Experiments were repeated twice with platelet-rich plasma (PRP) from each of the 2 patients with type 3 VWD, with similar results. The results shown are from the experiments with patient 2 PRP.

vitro and ex vivo. Because the velocity of clot formation in particular is anticipated to indirectly reflect the course of thrombin generation [16], our data suggest that rFVIII ameliorates platelet function throughout the entire blood hemostatic system via improved thrombin generation. To investigate these mechanisms further, we examined the effects of rFVIII on platelet function.

Activation of platelets by thrombin is essential for normal hemostasis, and thrombin plays a central role in cell-based hemostasis [2,17]. Platelet activation and blood coagulation are considered complementary and mutually dependent processes that are mediated by thrombin [18], and an investigation of the platelet response to thrombin would therefore provide insights into the role of FVIII in global hemostasis.

Tissue factor (TF)-mediated extrinsic coagulation occurs normally, even in the absence of both FVIII and VWF. Because TF-dependent thrombin generation is inhibited immediately by tissue factor pathway inhibitor (TFPI), however, the intrinsic coagulation pathway is critical for the response to subsequent hemostatic challenges. Hence, amplification of coagulation is normally mediated by positive-feedback mechanisms of the intrinsic pathway. Thus, at severely decreased FVIII levels, thrombin generation that is central to both primary and secondary hemostasis would be insufficient, regardless of the presence of VWF. These thrombin-induced aggregation studies using exogenous thrombin successfully helped in understanding the mechanisms involved downstream of thrombin generation mediated by TF and factor VIIa. In the current study, platelet aggregation was normalized by the addition of rFVIII in vitro and by rFVIII replacement ex vivo, suggesting the possibility that sufficient FVIII activity would adequately facilitate platelet activation in the absence of VWF through normalization of the intrinsic pathway.

Furthermore, in the SIPA studies rFVIII corrected the L-SIPA abnormality ex vivo. H-SIPA is mediated by VWF–glycoprotein Ib interactions and is considered to reflect platelet function related to the pathogenesis of arterial thrombosis rather than the events involved in normal hemostasis. Conversely, platelet aggregation induced under low shear is mediated by fibrinogen binding to the integrin $\alpha_{IIb}\beta_3$, and L-SIPA is thus more relevant to normal hemostasis and the pathogenesis of venous embolism than to the pathogenesis of platelet-arterial occlusion. In addition, $\alpha_{IIb}\beta_3$ can directly mediate the arrest of platelets on the vessel surface at relatively low shear rates [19]. Therefore, FVIII replacement can induce full platelet activation as well as evoke the coagulation system, thereby achieving normal hemostasis. Previous studies have demonstrated that exogenous FVIII binds to phospholipids of the platelet membrane, thereby contributing to the assembly of factor X–activating enzyme (Xase) on the platelet surface [20-22]. Our data are in keeping with these reports describing the importance of FVIII localized on the platelet membrane and consequently suggest the importance of platelet membrane–bound FVIII in the platelet-activation mechanism. The addition of rFVIII to PRP in vitro did not correct the defect, however. The reason for this discrepancy remains unclear. In the present study, however, FVIII may have been incorporated into the platelet membrane in vivo but failed to bind to the platelet surface in vitro, probably because of insufficient time or the absence of mechanical stimuli, such as flow and shear, needed for the incorporation of FVIII into platelets.

Of note was the effect of FVIII on platelet $[Ca^{2+}]_i$. Platelet activation by thrombin involves 2 receptors: high-affinity protease-activated receptor 1 (PAR-1) and low-affinity PAR-4 [23]. Lower concentrations of thrombin (<5 nM) predominantly induce cleavage of PAR-1 and $[Ca^{2+}]_i$ mobilization from intracellular stores with a distinctive profile. A PAR-4–dependent secondary mechanism involving adenosine diphosphate autocrine stimulation is required for prolonged Ca^{2+} responses. Higher concentrations of thrombin fully activate both PAR-1 and PAR-4. Thus, both PAR-1 and PAR-4 are implicated in the maximum activation of platelets [24,25]. In our studies, type 3 VWD platelets that were washed before rFVIII replacement responded only weakly, even to high concentrations of thrombin. After rFVIII replacement, both platelet aggregation and $[Ca^{2+}]_i$ mobilization in

response to thrombin were considerably enhanced. Again, a discrepancy between the in vitro assay and ex vivo assay was observed. The minor $[Ca^{2+}]_i$ changes initially seen in the absence of FVIII may lead to signal transduction but would not be sufficient to mediate adequate thrombin generation on the platelet surface. Two reasons have been advanced for the discrepancy, as in the case of the L-SIPA assay: insufficient time and the absence of mechanical stimuli. Because washed platelets were used in these assays, the improvements observed after rFVIII replacement were likely to have been the result of FVIII uptake by platelets; however, further investigations are needed to clarify this mechanism.

Taken together, these global and specific tests of hemostasis and platelet function indicate that exogenous FVIII was incorporated into the platelet membrane, facilitating platelet activation directly contributing to intrinsic coagulation. Although the presence of VWF is undoubtedly a prerequisite for optimum responses to a primary hemostatic challenge such as mucosal bleeding, clinical observations have shown that FVIII activity may be the only parameter that needs to be considered for the effective treatment of VWD [26,27]. This study further indicates that FVIII may promote adequate hemostatic control, even in the absence of VWF.

Acknowledgments

This work was supported in part by Health and Labour Sciences Research Grants for Research on HIV/AIDS from the Ministry of Health, Labour and Welfare. The authors are grateful to Dr. John C. Giddings for his critical reading of the manuscript. We are indebted to the patients and their families for their kind cooperation.

References

1. Sadler JE. A revised classification of von Willebrand disease: for the Subcommittee on von Willebrand Factor of the Scientific and Standardization Committee of the International Society on Thrombosis and Haemostasis. *Thromb Haemost.* 1994;71:520–525.
2. Hoffman M, Monroe DM 3rd. A cell-based model of hemostasis. *Thromb Haemost.* 2001;85:958–965.
3. Mannucci PM, Tamaro G, Narchi G, et al. Life-threatening reaction to factor VIII concentrate in a patient with severe von Willebrand disease and alloantibodies to von Willebrand factor. *Eur J Haematol.* 1987;39:467–470.
4. Bergamaschini L, Mannucci PM, Federici AB, Coppola R, Guzzoni S, Agostoni A. Posttransfusion anaphylactic reactions in a patient with severe von Willebrand disease: role of complement and alloantibodies to von Willebrand factor. *J Lab Clin Med.* 1995;125: 348–355.
5. Boyer-Neumann C, Dreyfus M, Wolf M, Veyradier A, Meyer D. Multi-therapeutic approach to manage delivery in an alloimmunized patient with type 3 von Willebrand disease. *J Thromb Haemost.* 2003;1:190–192.
6. Sakurai Y, Shima M, Imai Y, Omura S, Kirita T, Yoshioka A. Successful use of recombinant factor VIII devoid of von Willebrand factor during multiple teeth extractions in a patient with type 3 von Willebrand disease. *Blood Coagul Fibrin.* 2006;17:151–154.
7. Noe DA. A mathematical model of coagulation factor VIII kinetics. *Haemostasis.* 1996;26:289–303.
8. Vig S, Chitolie A, Bevan DH, Halliday A, Dormandy J. Thromboelastography: a reliable test? *Blood Coagul Fibrin.* 2001;12:555–561.
9. Mikhailidis DP, Barradas MA, Maris A, Jeremy JY, Dandona P. Fibrinogen mediated activation of platelet aggregation and thromboxane A2 release: pathological implications in vascular disease. *J Clin Pathol.* 1985;38:1166–1171.
10. Ikeda Y, Handa M, Kawano K, et al. The role of von Willebrand factor and fibrinogen in platelet aggregation under varying shear stress. *J Clin Invest.* 1991;87:1234–1240.
11. Sakurai Y, Fujimura Y, Kokubo T, et al. The cDNA cloning and molecular characterization of a snake venom platelet glycoprotein Ib-binding protein, mamushigin, from *Agkistrodon halys blomhoffii* venom. *Thromb Haemost.* 1998;79:1199–1207.
12. Pollock WK, Rink TJ. Thrombin and ionomycin can raise platelet cytosolic Ca^{2+} to micromolar levels by discharge of internal Ca^{2+} stores: studies using fura-2. *Biochem Biophys Res Commun.* 1986; 139:308–314.
13. Grynkiewicz G, Poenie M, Tsein RY. A new generation of Ca^{2+} indicators with greatly improved fluorescence properties. *J Biol Chem.* 1985;260:3440–3450.
14. Kasuda S, Sakurai Y, Shima M, et al. Inhibition of PAR4 signaling mediates ethanol-induced attenuation of platelet function in vitro. *Alcohol Clin Exp Res.* 2006;30:1608–1614.
15. Calatzis A, Haas S, Gödje O, Calatzis A, Hipp R, Walenga J. Thromboelastographic coagulation monitoring during cardiovascular surgery with the ROTEG coagulation analyzer. In: Pifarré R, ed. *Management of Bleeding in Cardiovascular Surgery.* Philadelphia, Pa: Hanley & Belfus; 2000:215–226.
16. Sørensen B, Johansen P, Christiansen K, Woelke M, Ingerslev J. Whole blood coagulation thrombelastographic profiles employing minimal tissue factor activation. *J Thromb Haemost.* 2003;1:551–558.
17. Sambrano GR, Weiss EJ, Zheng YW, Huang W, Coughlin SR. Role of thrombin signalling in platelets in haemostasis and thrombosis. *Nature.* 2001;413:74–78.
18. Heemskerk JW, Bevers EM, Lindhout T. Platelet activation and blood coagulation. *Thromb Haemost.* 2002;88:186–193.
19. Savage B, Saldivar E, Ruggeri ZM. Initiation of platelet adhesion by arrest onto fibrinogen or translocation on von Willebrand factor. *Cell.* 1996;84:289–297.
20. Berndt MC, Gregory C, Dowden G, Castaldi PA. Thrombin interactions with platelet membrane proteins. *Ann N Y Acad Sci.* 1986; 485:374–386.
21. Yoshioka A, Peake IR, Furlong BL, Furlong RA, Giddings JC, Bloom AL. The interaction between factor VIII clotting antigen (VIIICAg) and phospholipid. *Br J Haematol.* 1983;55:27–36.
22. Muntean W, Leschnik B, Haas J. Factor VIII coagulant moiety binds to platelets by binding to phospholipids of the platelet membrane. *Thromb Res.* 1987;45:345–354.
23. Kahn ML, Zheng YW, Huang W, et al. A dual thrombin receptor system for platelet activation. *Nature.* 1998;394:690–694.
24. Kahn ML, Nakanishi-Matsui M, Shapiro MJ, Ishihara H, Coughlin SR. Protease-activated receptors 1 and 4 mediate activation of human platelets by thrombin. *J Clin Invest.* 1999;103:879–887.
25. Covic L, Gresser AL, Kuliopulos A. Biphasic kinetics of activation and signaling for PAR1 and PAR4 thrombin receptors in platelets. *Biochemistry.* 2000;39:5458–5467.
26. Federici AB, Mannucci PM. Optimizing therapy with factor VIII/von Willebrand factor concentrates in von Willebrand disease. *Haemophilia.* 1998;4(suppl 3):7–10.
27. Castaman G, Federici AB, Rodeghiero F, Mannucci PM. Von Willebrand's disease in the year 2003: towards the complete identification of gene defects for correct diagnosis and treatment. *Haematologica.* 2003;88:94–108.

Tissue-Targeted In Vivo Gene Transfer Coupled with Histone Deacetylase Inhibitor Depsipeptide (FK228) Enhances Adenoviral Infection in Rat Renal Cancer Allograft Model Systems

Minoru Kobayashi, Takashi Okada, Takashi Murakami, Keiya Ozawa, Eiji Kobayashi, and Tatsuo Morita

OBJECTIVES Although the adenoviral vector represents an efficient delivery system, hepatotropic accumulation often has detrimental effects on adenoviral vector-mediated cancer therapy. To overcome this disadvantage, we performed in vivo local gene transfer, in combination with the histone deacetylase inhibitor, depsipeptide (FK228), in a rat renal cancer model.

METHODS Renal cancer cells induced by ferric nitrilotriacetate in ACI rats were used in this study. Adenoviral vectors containing luciferase cDNA were introduced into the tumor-burdened kidney by way of a catheter placed in the renal artery. Subcutaneous tumors were treated by herpes simplex virus thymidine kinase cDNA followed by intraperitoneal ganciclovir. The levels of Coxsackie-adenovirus receptor in various tissue were determined by quantitative reverse transcriptase-polymerase chain reaction. Depsipeptide (1 mg/kg) was intravenously administered 24 hours before adenoviral vector transduction.

RESULTS The catheter-based adenoviral vector delivery enabled strong gene transduction of the tumor-burdened kidney. Moreover, depsipeptide treatment before adenoviral vector injection significantly improved transgene expression at tumor sites. Quantitative reverse transcriptase-polymerase chain reaction analysis showed that depsipeptide increased the expression levels of the Coxsackie-adenovirus receptor in the renal tumor (13-fold), but not in other normal tissues. Furthermore, the use of herpes simplex virus thymidine kinase cDNA-expressing adenoviral vector followed by ganciclovir markedly inhibited the established tumor growth in combination with depsipeptide compared with herpes simplex virus thymidine kinase cDNA alone.

CONCLUSIONS The tissue-targeted in vivo gene transfer coupled with depsipeptide significantly enhanced adenoviral infection at tumor sites. Sensitization of tumor cells with depsipeptide can improve the efficacy of adenoviral vector-mediated suicide gene therapy. Thus, application of depsipeptide could be one of the beneficial adjunct for adenoviral vector-mediated cancer gene therapy. UROLOGY 70: 1230–1236, 2007. © 2007 Elsevier Inc.

Renal cell carcinoma (RCC) is a potentially mortal kidney disease. Surgical resection represents the therapeutic mainstay for localized RCC. However, one third of patients with RCC present with metastasis, and one half of patients treated for a localized primary tumor subsequently develop metastatic disease.[1] In particular, primary tumors that cannot be surgically removed (eg, solitary kidney, renal insufficiency, or bilateral tumors) are the most complicated forms of RCC. Antitumor cytokines such as interferon-alpha and interleukin-2 have been widely used, only to lead to limited therapeutic benefits.[2] Thus, a more tumor-selective targeting strategy is required for clinical RCC therapy.

Recent advances in cancer therapy have involved the use of the adenoviral vector, which has been widely applied in clinical cancer therapy for its high transduction efficiency. Because systemic adenoviral vector injection results in preferential accumulation in the liver owing to the hepatocytic tropism[3] and can induce unde-

From the Department of Urology, and Divisions of Genetic Therapeutics and Organ Replacement Research, Center for Molecular Medicine, Jichi Medical University, Tochigi, Japan; and Department of Molecular Therapy, National Institute of Neuroscience, National Center of Neurology and Psychology, Tokyo, Japan

Reprint requests: Minoru Kobayashi, M.D., Department of Urology, Jichi Medical University, 3311-1 Yakushiji, Shimotsuke, Tochigi 329-0498 Japan. E-mail: minoruk@jichi.ac.jp

Submitted: May 16, 2007, accepted (with revisions): September 14, 2007

0090-4295/07/$32.00
doi:10.1016/j.urology.2007.09.022

sirable immune responses to viral proteins,[4] adenoviral vector-mediated cancer therapy has been limited to the intratumor injection approach. However, this approach is not available if the tumor is located in inaccessible sites or if the tumor has spread extensively in the target organ. Therefore, it is necessary to use a more selective tissue-targeting strategy for adenoviral vector delivery.

Improving the efficiency of gene transduction will help to reduce adenoviral vector-mediated toxicity by decreasing the required quantity of viral vectors. It has been shown that histone deacetylase inhibitors (HDACis) can reactivate virally transduced genes[5] and modulate their expression at transcriptional levels.[6] The novel class of histone deacetylase inhibitors, depsipeptide (FK228, FR901228), which was originally developed as an anticancer agent, has been shown to augment adenoviral vector-mediated transgene expression in various tumor cell lines in vitro.[7–9] However, little is known about the in vivo effect of depsipeptide on enhancing gene expression[10–12] or the adenoviral vector distribution defining the tissues in vivo, where the vectors spread.

We have demonstrated that tissue-targeted local gene transfer using the catheter-based technique overcomes the adenoviral hepatocytic tropism in a rat orthotopic RCC model. Moreover, depsipeptide-mediated sensitization increases the efficiency of adenoviral vector-mediated in vivo gene transfer in a tumor-selective manner. The mechanism for increasing transgene expression in the tumor was also evaluated in relation to Coxsackie-adenovirus receptor (CAR) expression; the CAR serves as a high-affinity receptor for adenoviral vectors and adenovirus type 5.[13]

MATERIAL AND METHODS

Animals, Cells, and Reagents

Male inbred ACI rats (6 to 8 weeks old) were purchased from CLEA Japan (Tokyo, Japan). All experiments were performed in accordance with the Jichi Medical University Guide for Laboratory Animals. Rat renal cancer cells had been previously established from an ACI rat exposed to ferric nitrilotriacetate[14] and were maintained in vivo in the subcutaneous space of ACI rats every 2 weeks. Depsipeptide was obtained from Fujisawa Pharmaceutical (Osaka, Japan).

Adenovirus Vectors

We constructed a replication-deficient adenoviral vectors (serotype 5 with E1/E3 deletion) containing firefly luciferase cDNA (AVC2-luc) or herpes simplex virus thymidine kinase cDNA (AVC2-tk) driven under cytomegalovirus promoter, using the in vitro ligation technique with DNA protein complex.[15] The adenoviral vectors were purified by sequential CsCl step gradients and isopycnic centrifugation and then titered by determination of the median tissue culture infection dose. The LacZ (beta-galactosidase)-expressing adenoviral vector AxCA-LacZ, driven by chicken beta-actin promoter and cytomegalovirus enhancer, was donated by Dr. Xiao-Kang Li (Department of Regeneration Surgery, National Research Institute for Child Health and Development, Tokyo, Japan).[16]

In Vivo Luminescent Imaging and 5-Bromo-4-Chloro-3-Iodolyl-β-D-Galactopyranoside Staining

In vivo luciferase imaging was conducted with the noninvasive bioimaging system IVISTM (Xenogen, Alameda, Calif). One minute after an intravenous injection of D-luciferin (30 mg/kg) (potassium salt, Biosynth, Postfach, Switzerland), the signal intensity of the emitted photons from the luciferase-expressing tissue were measured with 1 minute of integration time. To visualize the LacZ expression, frozen sections were stained with chromogenic substrate 5-bromo-4-chloro-3-iodolyl-β-D-galactopyranoside using a previously described procedure.[17]

Tumor Models and Suicide Gene Therapy

For the subcutaneous tumor model, harvested tumor cells (4×10^5) were injected into the abdominal subcutaneous space of the rats. The tumor volume was evaluated using the following equation: tumor volume = (length in millimeters) × (width in millimeters)^2/2. For the orthotopic tumor model of the kidney, the cells (1×10^6) were suspended in 0.1 mL phosphate-buffered saline and inoculated into the left renal subcapsular space. An obvious subcapsular tumor was established about 1 week later. For suicide gene therapy, AVC2-tk (1.5×10^9 pfu) was injected into the subcutaneous tumor, followed by continuous intraperitoneal infusion of ganciclovir (GCV) (240 mg/kg/day) for 7 consecutive days using a miniosmotic pump (Alzet, Palo Alto, Calif) according to the manufacturer's instructions. Tumor growth was monitored every other day with tumor volume measurements.

Catheter-Based In Vivo Gene Transfer

Catheter-based gene transfer was performed using a previously described method[18] on the iliac artery and a 2F catheter (Solo-Cath, Solomon Scientific, Plymouth Meeting, Pa) was passed through to the abdominal aorta just distal to the origin of the left renal artery. After the aorta was clamped just proximal to the left renal artery, 2 mL of saline was injected by way of the catheter to wash out blood in the tissue, followed by 1 mL of phosphate-buffered saline containing adenoviral vector (5×10^8 pfu of AVC2-luc or 1×10^9 pfu of AxCA-LacZ). The left renal artery and vein were clamped for 10 minutes to allow tissue contact with the injected adenoviral vector.

Quantitative Real-Time Reverse Transcriptase-Polymerase Chain Reaction

Total RNA was extracted from rat tissues using RNA-Bee reagent (Cosmo Bio, Tokyo, Japan). Total RNA (1.5 μg) was used for first-strand synthesis of cDNA using the SuperScript Preamplification System (Invitrogen, Carlsbad, Calif) and amplified using QuantiTect SYBR Green polymerase chain reaction (PCR) (Qiagen, Valencia, Calif). The following PCR primers were used: CAR forward, 5′-CTGATCAGTGTATGCTAC GACTAGATGTT-3′; CAR reverse, 5′-CAAGCAGCGTCCCTATGACA-3′; glyceraldehyde-3-phosphate dehydrogenase (GAPDH) forward, 5′-GACAAC TTTGGCATCGTGGA-3′; and GAPDH reverse, 5′-ATGCAGGGATGATGTTCTGG-3′. The PCR product was analyzed using the ABI PRISM 7900 HT Sequence Detection System (Applied Biosystems, Foster City, Calif). Quantitative values were obtained from the threshold cycle (C_t) number that indicated exponential amplification of the PCR product. The relative CAR expression level was determined as the N-fold

difference relative to GAPDH according to the following formula: $N = 2^{\text{corrected } \Delta C_t \text{ (GAPDH - CAR)}}$. The C_t value was determined by subtracting the average CAR C_t value from that of GAPDH. Each experiment was performed two to three times with similar results.

Statistical Analysis

P values were obtained through Student's *t* test or the Mann-Whitney *U* test using the StatView software (Abacus Concepts, Berkeley, Calif). Data are shown as the mean ± standard deviation. Differences between groups were considered significant at $P < 0.05$.

RESULTS

In Vivo Adenoviral Vector Distribution After Systemic Injection

To examine the distribution of systemically injected adenoviral vector in vivo, luciferase-expressing adenoviral vectors (5×10^8 pfu) were injected intravenously. Vector distribution was monitored by in vivo luciferase imaging (Fig. 1A). The vector-derived photons accumulated exclusively in the spleen and liver at day 2 after adenoviral vector injection, and these organs were substantially luciferase positive in the ex vivo analysis (Fig. 1B).

In Vivo Gene Transfer in Tumor-Burdened Kidneys of Rats

Because systemic adenoviral vector injection did not result in substantial transgene expression at the tumor sites, it was necessary to use a more selective strategy for tumor-specific targeting. In our previous work, we demonstrated a catheter-based in vivo gene delivery method that potentially allows for kidney-selective adenoviral vector transfer.[18] We, therefore, applied this catheter-based technique to target the orthotopic RCC tumor in the rat model. The catheter-based injection of luciferase-expressing adenoviral vector showed strong transgene expression in the kidney (Fig. 1C), in which rat RCC cells were transplanted beneath the renal capsule (Fig. 1D). Moreover, to determine whether catheter-based adenoviral vector gene transfer is an effective technique for tumor targeting, beta-galactosidase-expressing adenoviral vectors (1×10^9 pfu) were administered into the left kidney of the rats using a catheter, and the tissue was analyzed using an 5-bromo-4-chloro-3-iodolyl-β-D-galactopyranoside staining procedure. As shown in Figure 1E, beta-galactosidase expression was dominant in the tumor area and around the boundary of the renal parenchyma. Thus, these results suggest that catheter-based adenoviral vector gene delivery might be an effective technique for tumor targeting in the kidney.

Effect of Depsipeptide Pretreatment on Adenoviral Vector-Mediated Tumor Targeting

Recent evidence has shown that transcriptional modulation using HDACis can augment adenoviral vector-mediated gene expression in various tumor cells in vitro. Therefore, we hypothesized that the use of an HDACi might improve the efficiency of adenoviral vector-mediated tumor destruction in vivo. To address whether the HDACi depsipeptide enhances adenoviral vector-derived transgene expression in tumors, AVC2-luc (5×10^8 pfu) was injected directly into subcutaneous tumors 24 hours after intravenous injection of depsipeptide (1 mg/kg). This dosage and timing of depsipeptide was preliminary determined to be optimal to show maximal transgene expression in the subcutaneous tumor model (data not shown). Depsipeptide pretreatment significantly enhanced luciferase gene expression in the tumor compared with the mock treatment, and substantial photons were observed from day 1 to day 5 after adenoviral vector transduction (Fig. 2A). A similar enhancement of gene expression was also observed in the orthotopically transplanted RCC tumor subjected to local AVC2-luc transfer using the catheter-based method (Fig. 2B). Although adenoviral vector-derived photons in the liver were observed faintly even when using the catheter-based targeting procedure, depsipeptide treatment did not result in an additional increase of adenoviral vector-derived photons in the liver or any other normal tissues (data not shown). Thus, these findings suggest that depsipeptide modulates transgene expression in a tumor-selective manner.

Upregulation of Adenoviral Vector Receptor CAR in Tumors by Depsipeptide

As shown in recent studies,[7,8,11,12] we investigated whether in vivo exposure of RCC cells with depsipeptide can increase CAR expression levels, which consequently involves enhancement of adenoviral vector transduction in our model systems. CAR mRNA expression in various tissues and subcutaneous tumor was examined after 24 hours with or without depsipeptide injection (1 mg/kg). Depsipeptide treatment strikingly enhanced CAR expression in the tumor (13-fold increase relative to untreated tumor) but had no such effect on normal, healthy tissues (Fig. 2C). These results explain that depsipeptide sensitizes RCC tumors for adenoviral vector-mediated gene therapy partly through an increase in CAR levels.

Use of Depsipeptide Enhances Tumor-Selective Suicide Gene Therapy in Rat Model

Finally, we investigated whether sensitization of the RCC tumor with depsipeptide promoted herpes simplex virus thymidine kinase cDNA-mediated tumor transduction. Herpes simplex virus thymidine kinase cDNA-expressing adenoviral vectors (AVC2-tk, 1.5×10^9 pfu) were injected into an established subcutaneous tumor with or without depsipeptide treatment (1 mg/kg) 48 hours before intraperitoneal GCV injection. As shown in Figure 2D, the use of depsipeptide before adenoviral vector-mediated suicide therapy with AVC2-tk and GCV significantly decreased the tumor size compared

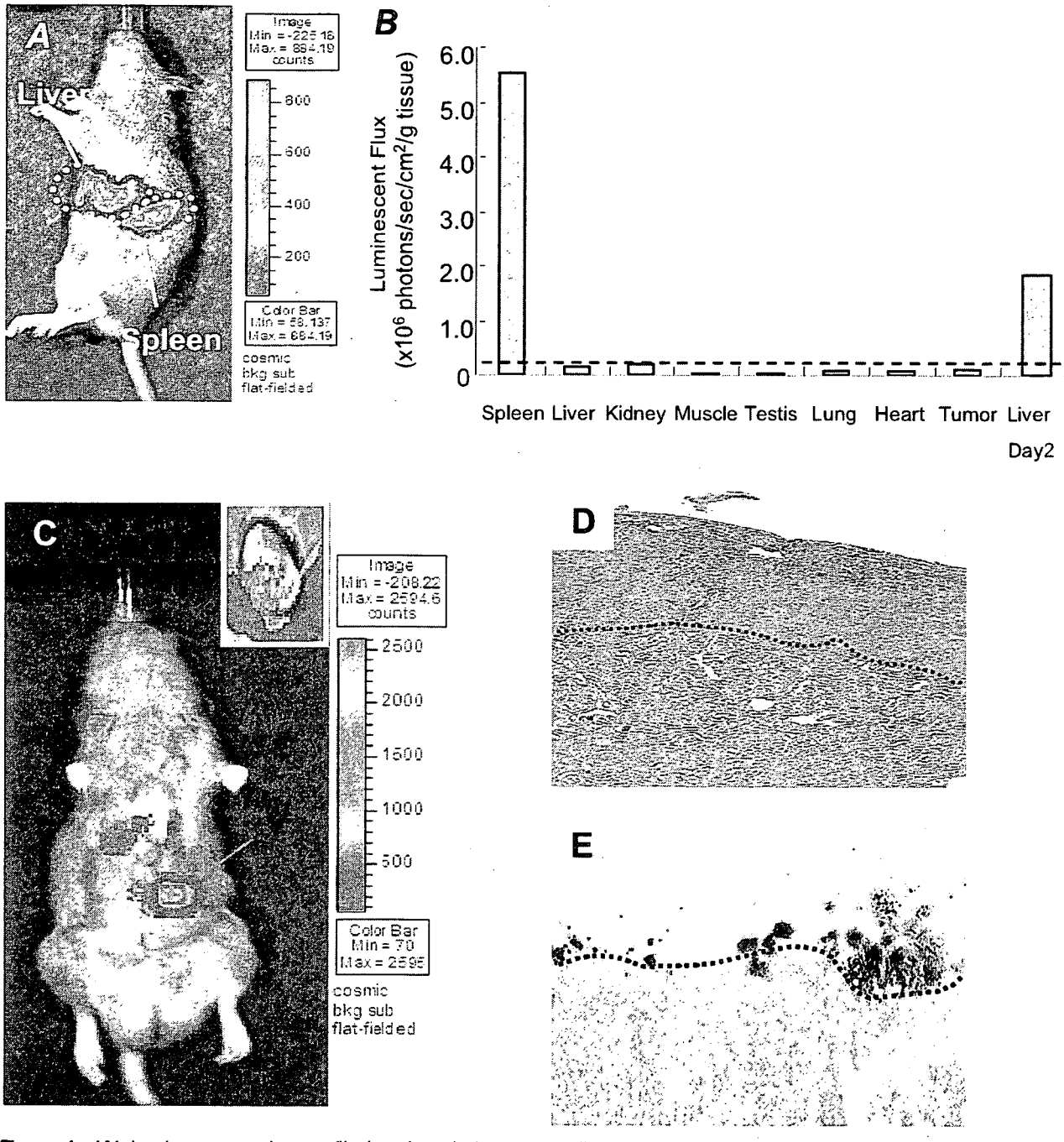

Figure 1. (A) In vivo expression profile in adenoviral vector-mediated gene transfer. Optical bioluminescent imaging of adenoviral vector-mediated gene transfer. AVC2-luc (5×10^8 pfu) injected intravenously and luciferase images taken at day 2 after transduction. Substantial photons detected in spleen and liver. **(B)** Ex vivo analysis of luciferase expression from various tissues of ACI rat. Tissues isolated at day 1 or day 2 after systemic AVC2-luc injection. Luciferase expression detected exclusively in spleen and liver. Dotted line represents background level (in tissues of control rats). **(C)** Successful catheter-based in vivo adenoviral vector delivery into orthotopic renal tumor of rats. Representative image of luciferase transduction after injection of AVC2-luc (5×10^8 pfu). Luciferase images obtained at day 2 after adenoviral vector transduction. Red arrow indicates left kidney. Inset shows ex vivo luciferase analysis of isolated tumor-burdened kidney. Photons detected macroscopically in subcapsular area of kidney. **(D)** Representative histologic section of established subcapsular tumor of kidney. Dotted line indicates border of parenchyma. Hematoxylin-eosin stain, original magnification ×20. **(E)** Expression pattern of LacZ after catheter-based adenoviral vector transfer. Beta-galactosidase expression evaluated by 5-bromo-4-chloro-3-iodolyl-β-D-galactopyranoside staining of tumor-burdened kidney of rats (blue area). LacZ-positive cells predominantly stained blue in subcapsular tumor area. Dotted line indicates border of parenchyma. Original magnification ×40.